

1 **Source-Resolved Volatility and Oxidation State Decoupling in**
2 **Wintertime Organic Aerosols in Seoul**

3
4 Hwajin Kim^{1,2,*}, Jiwoo Jeong¹, Jihye Moon¹, Hyun Gu Kang^{2,3}

5 ¹Department of Environmental Health Sciences, Graduate School of Public Health, Seoul National University, 08826 Seoul,
6 South Korea

7 ²Institute of Health and Environment, Graduate School of Public Health, Seoul National University, 08826 Seoul, South Korea

8 ³Now at Multiphase Chemistry Department, Max Planck Institute for Chemistry, 55128 Mainz, Germany

9 *Correspondence to:* Hwajin Kim (khj0116@snu.ac.kr)

10 **Abstract.**

11 Organic aerosols (OA) are key components of wintertime urban haze, but the relationship between their oxidation
12 state and volatility—critical for understanding aerosol evolution and improving model predictions—remains poorly
13 constrained. While oxidation–volatility decoupling has been observed in laboratory studies, field-based evidence
14 under real-world conditions is scarce, particularly during severe haze episodes. This study presents a field-based
15 investigation of OA sources and their volatility characteristics in Seoul during a winter haze period, using a
16 thermodenuder coupled with a high-resolution time-of-flight aerosol mass spectrometer (HR-ToF-AMS).

17 Positive matrix factorization resolved six OA factors: hydrocarbon-like OA, cooking, biomass burning, nitrogen-
18 containing OA (NOA), less-oxidized oxygenated OA (LO-OOA), and more-oxidized OOA (MO-OOA). Despite
19 having the highest oxygen-to-carbon ratio (~1.15), MO-OOA exhibited unexpectedly high volatility, indicating a
20 decoupling between oxidation state and volatility. We attribute this to fragmentation-driven aging and autoxidation
21 under stagnant conditions with limited OH exposure. In contrast, LO-OOA showed lower volatility and more
22 typical oxidative behavior.

23 Additionally, NOA—a rarely resolved factor in wintertime field studies—was prominent during cold, humid, and
24 stagnant conditions and exhibited chemical and volatility features similar to biomass burning OA, suggesting a
25 shared combustion origin and meteorological sensitivity.

26 These findings provide one of the few field-based demonstrations of oxidation–volatility decoupling in ambient
27 OA and highlight how source-specific properties and meteorology influence OA evolution. The results underscore
28 the need to refine OA representation in chemical transport models, especially under haze conditions.

29 **Keywords:** Organic aerosol volatility, HR-ToF-AMS, Thermodenuder, elemental ratios, aging, fragmentation

30 **1 Introduction**

31 Atmospheric aerosols affect both human health and the environment by reducing visibility (Ghim et al., 2005; Zhao
32 et al., 2013) and contributing to cardiovascular and respiratory diseases (Hamanaka et al., 2018; Manalisidis et al.,
33 2020). In addition, aerosols play a significant role in climate change by scattering or absorbing solar radiation and
34 modifying cloud properties (IPCC AR6). Among the various aerosol components—including sulfate, nitrate,
35 ammonium, chloride, crustal materials, and water—organic aerosols (OA) are particularly important to characterize,
36 as they account for 20–90% of submicron particulate matter (Zhang et al., 2007). Identifying OA sources and
37 understanding their behavior are critical for effective air quality management; however, this is particularly
38 challenging due to the vast diversity and dynamic nature of OA compounds, which originate from both natural and
39 anthropogenic sources. Unlike inorganic aerosols, organic aerosols (OAs) evolve continuously through complex
40 atmospheric reactions, influenced by emission sources, meteorological conditions, and aerosol properties (Jimenez
41 et al., 2009; Hallquist et al., 2009; Robinson et al., 2007; Donahue et al., 2006; Ng et al., 2010; Cappa and Jimenez,
42 2010).

43 Volatility is a key parameter for characterizing organic aerosol (OA) properties, as it governs gas-to-particle
44 partitioning behavior and directly influences particle formation yields (Sinha et al., 2023). The classification of OA
45 species based on their volatility—from extremely low-volatility (ELVOC) to semi-volatile (SVOC) and
46 intermediate-volatility (IVOC) compounds—is central to the conceptual framework of secondary OA (SOA)
47 formation and growth (Donahue et al., 2006). It also affects atmospheric lifetimes and human exposure by
48 determining how long aerosols remain suspended in the atmosphere (Glasius and Goldstein, 2016). Therefore,
49 accurately capturing OA volatility is essential for improving predictions of OA concentrations and their
50 environmental and health impacts. However, chemical transport models often significantly underestimate OA mass
51 compared to observations (Jiang et al., 2012; Li et al., 2017), largely due to incomplete precursor inventories and
52 simplified treatment of processes affecting OA volatility. For instance, aging—through oxidation reactions such as
53 functionalization and fragmentation—can significantly alter volatility by changing OA chemical structure
54 (Robinson et al., 2007; Zhao et al., 2016). Early volatility studies primarily utilized thermal denuders (TD) coupled
55 with various detection instruments to investigate the thermal properties of bulk OA (Huffman et al., 2008). The
56 subsequent coupling of TD with the Aerosol Mass Spectrometer allowed for component-resolved volatility
57 measurements, providing critical, quantitative insight into the properties of OA factors (e.g., SV-OOA vs. LV-
58 OOA) across different regions (Paciga et al., 2016; Cappa and Jimenez, 2010). These component-resolved volatility
59 data are often used to constrain the Volatility Basis Set (VBS)—the current state-of-the-art framework for

60 modeling OA partitioning and evolution (Donahue et al., 2006). However, a limitation in many field studies is that
61 the TD-AMS thermogram data are rarely translated into quantitative VBS distributions for individual OA factors,
62 which limits their direct use in chemical transport models. Furthermore, the volatility of OOA during extreme haze
63 conditions, where the expected inverse correlation between oxidation (O:C) and volatility can break down (Jimenez
64 et al., 2009), remains poorly characterized, particularly in East Asia's highly polluted winter environments. A recent
65 study in Korea further highlighted the importance of accounting for such processes when interpreting OA volatility
66 under ambient conditions (Kang et al., 2022). Given its central role in OA formation, reaction, and atmospheric
67 persistence, volatility analysis is critical for bridging the gap between measurements and model performance.

68 Traditionally, due to the complexity and variability of OA, the oxygen-to-carbon (O:C) ratio has been used as a
69 proxy for estimating volatility. In general, higher O:C values indicate greater oxidation and lower volatility
70 (Jimenez et al., 2009). Accordingly, many field studies classify oxygenated OA (OOA) into semi-volatile OOA
71 (SV-OOA) and low-volatility OOA (LV-OOA) based on their O:C ratios (Ng et al., 2010; Huang et al., 2010; Mohr
72 et al., 2012). However, this relationship is not always straightforward. Fragmentation during oxidation can increase
73 both O:C and volatility simultaneously, disrupting the expected inverse correlation (Jimenez et al., 2009). In
74 laboratory experiments, yields of highly oxidized SOA have been observed to decrease due to fragmentation (Xu
75 et al., 2014; Grieshop et al., 2009). These findings suggest that while O:C can offer useful insights, it is insufficient
76 alone to represent OA volatility. Direct volatility measurements, especially when paired with chemical composition
77 data, are necessary to improve our understanding of OA sources and aging processes.

78 In this study, we investigate the sources and volatility characteristics of OA in Seoul during winter. Wintertime OA
79 presents additional challenges due to its high complexity. During winter, emissions from combustion sources such
80 as biomass burning and residential heating significantly increase, contributing large amounts of primary OA (Kim
81 et al., 2017). Meanwhile, low ambient temperatures and reduced photochemical activity affect the formation and
82 evolution of secondary OA (SOA). Frequent haze events further complicate the aerosol properties by extending
83 aging times and increasing particle loadings. These overlapping sources and atmospheric conditions make winter
84 OA particularly difficult to characterize and predict. Despite Seoul's significance for air quality management,
85 comprehensive studies on OA volatility during winter remain limited. To address these goals, we conducted real-
86 time, high-resolution measurements using a high-resolution time-of-flight aerosol mass spectrometer (HR-ToF-
87 AMS) coupled with a thermodenuder (TD). The objectives of this study are to: (1) improve the understanding of

88 wintertime OA in Seoul, (2) characterize the volatility of OA associated with different sources, and (3) explore the
89 relationship between OA volatility and chemical composition.

90 **2 Experimental methods**

91 **2.1 Sampling Site and Measurement Period**

92 We conducted continuous real-time measurements in Seoul, South Korea, from 28 November to 28 December
93 2019. The sampling site was located in the northeastern part of the city (37.60° N, 127.05° E), approximately 7 km
94 from the city center, surrounded by major roadways and mixed commercial–residential land use. Air samples were
95 collected at an elevation of approximately 60 meters above sea level, on the fifth floor of a building. A detailed site
96 description has been reported previously for winter Seoul (Kim et al., 2017). During this period, the average
97 ambient temperature was $1.76 \pm 4.3^{\circ}$ C, and the average relative humidity (RH) was $56.9 \pm 17.5\%$, based on data
98 from the Korea Meteorological Administration (<http://www.kma.go.kr>).

99 **2.2 Instrumentation and Measurements**

100 The physico-chemical properties of non-refractory PM_1 (NR- PM_1) species—including sulfate, nitrate, ammonium,
101 chloride, and organics—were measured using an Aerodyne high-resolution time-of-flight aerosol mass
102 spectrometer (HR-ToF-AMS) (DeCarlo et al., 2006). PM_1 mass in this study is taken as NR- PM_1 (from AMS) +
103 black carbon (BC; measured by MAAP), which is appropriate for winter Seoul where refractory PM_1 (metal/sea-
104 salt/crustal) is minor and dust events were excluded (e.g., Kim et al., 2017; Nault et al., 2018; Kang et al., 2022;
105 Jeon et al., 2023). Data were acquired at 2.5-minute intervals, alternating between V and W modes. The V mode
106 provides higher sensitivity but lower resolution, suitable for mass quantification, whereas the W mode offers higher
107 mass resolution but lower sensitivity, used here for OA source apportionment. Simultaneously, black carbon (BC)
108 concentrations were measured at 1-minute intervals using a multi-angle absorption photometer (MAAP; Thermo
109 Fisher Scientific, Waltham, MA, USA). Total PM_1 mass was calculated as the sum of NR- PM_1 and BC.

110 Hourly trace gas concentrations (CO, O₃, NO₂, SO₂) were obtained from the Gireum air quality monitoring station
111 (37.61° N, 127.03° E), managed by the Seoul Research Institute of Public Health and Environment. Meteorological

112 data (temperature, RH, wind speed/direction) were collected from the nearby Jungreung site (37.61° N, 127.00°
113 E). All data are reported in Korea Standard Time (UTC+9).

114 To examine aerosol volatility, a thermodenuder (TD; Envalytix LLC) was installed upstream of the HR-ToF-AMS.
115 Details are provided in Supplementary Section S1 Kang et al. (2022). Briefly, ambient flow alternated every 5
116 minutes between a TD line and a bypass line at 1.1 L min^{-1} . Residence time in the TD line was $\sim 6.3 \text{ s}$. The TD
117 setup included a 50 cm heating section followed by an adsorption unit. Heated particles were stripped of volatile
118 species, while the downstream carbon-packed section prevented recondensation. TD temperature cycled through
119 12 steps (30 to 200 °C), with each step lasting 10 min (total cycle = 120 min). AMS V and W modes were alternated
120 during the same cycle. The heater was pre-adjusted to the next temperature while the bypass was active.

121

122 **2.3 Data Analysis**

123

124 **2.3.1 Data analysis and OA Source Apportionment**

125 HR-AMS data were processed using SQUIRREL v1.65B and PIKA v1.25B. Mass concentrations of non-refractory
126 PM₁ (NR-PM₁) species were derived from V-mode data, while high-resolution mass spectra (HRMS) and the
127 elemental composition of organic aerosols (OA) were obtained from W-mode data. NR-PM₁ quantification
128 followed established AMS protocols (Ulbrich et al., 2009; Zhang et al., 2011). Both the bypass and TD streams
129 were processed using a time-resolved, composition-dependent collection efficiency CE(t) following Middlebrook
130 et al. (2012). TD heating can modify particle water and phase state/mixing and thereby influence CE beyond
131 composition (Huffman et al., 2009), but prior TD-AMS studies indicate that such effects are modest and largely
132 multiplicative, which do not distort thermogram shapes or T₅₀ ordering (Faulhaber et al., 2009; Cappa & Jimenez,
133 2010). In our data, the CE(t) statistics for the two lines were similar (campaign-average CE: TD = 0.55 ± 0.08 ;
134 bypass = 0.53 ± 0.04 ; $\Delta = 0.02 \approx 3.7\%$, below the combined uncertainty ≈ 0.09). We therefore report volatility
135 metrics with these line-specific CE(t) corrections applied and interpret potential residual CE effects as minor. For
136 organics, elemental ratios (O:C, H:C, and OM/OC) were calculated using the Improved-Ambient (IA) method
137 (Canagaratna et al., 2015). Positive Matrix Factorization (PMF) was applied to the HRMS of organics using the
138 PMF2 algorithm (v4.2, robust mode) (Paatero and Tapper, 1994). The HRMS and corresponding error matrices
139 from PIKA were analyzed using the PMF Evaluation Tool v2.05 (Ulbrich et al., 2009). Data pretreatment followed
140 established protocols (Ulbrich et al., 2009; Zhang et al., 2011). A six-factor solution (fPeak = 0; Q/Q_expected =
141 3.56) was selected as optimal (Fig. S1). The resolved OA sources included hydrocarbon-like OA (HOA; 14%; O:C

142 = 0.13), cooking-related OA (COA; 21%; O:C = 0.18), nitrogen-enriched OA (NOA; 2%; O:C = 0.22), biomass-
143 burning OA (BBOA; 13%; O:C = 0.25), less-oxidized oxygenated OA (LO-OOA; 30%; O:C = 0.68), and more-
144 oxidized oxygenated OA (MO-OOA; 20%; O:C = 1.15) (Figs. S2 and S3). Alternative five- and seven-factor
145 solutions were also evaluated. In the five-factor solution, the biomass burning source was not clearly resolved and
146 appeared to be distributed across multiple factors. In the seven-factor solution, BBOA was further split into two
147 separate factors without clear distinction or added interpretive value, making the six-factor solution the most
148 physically meaningful and interpretable (Figs. S4 and S5). To ensure the statistical robustness of this solution, we
149 calculated uncertainties for each PMF factor using the bootstrap method (100 iterations) with the PET toolkit
150 (v2.05) (EPA, 2014; Xu et al., 2018; Srivastava et al., 2021) (Table S2 and Fig. S13).

151

152 **2.3.2 Thermogram and Volatility Estimation**

153 The chemical composition dependent mass fraction remaining (MFR) was derived at each TD temperature by
154 dividing the corrected mass concentration of the TD line [p] by the average of the adjacent bypass lines [p-1] and
155 [p+1]. Thermograms were corrected for particle loss, estimated using reference substances like NaCl, which exhibit
156 minimal evaporation (Huffman et al., 2009; Saha et al., 2014; Kang et al., 2022). OA factor concentrations at each
157 TD temperature were derived via multivariate linear regression between post-TD HRMS and ambient OA factor
158 HRMS profiles as described in Zhou et al., 2017.

159 Volatility distributions were modeled using the thermodenuder mass transfer model from Riipinen et al. (2010) and
160 Karnezi et al. (2014), implemented in Igor Pro 9 (Kang et al., 2022). OA mass was distributed into eight logarithmic
161 saturation concentration bins (C^* : 1000 to $0.0001 \mu\text{g m}^{-3}$). Modeled MFRs were fit to observations using Igor's
162 "FuncFit" function, repeated 1,000 times per OA factor to determine best-fit results. The model assumes no thermal
163 decomposition and includes adjustable parameters: mass accommodation coefficient (α_m) and enthalpy of
164 vaporization (ΔH_{exp}), randomly sampled within literature-based ranges (Table S1).

165

166 **3 Results and discussion**

167 **3.1 Overview of PM₁ Composition and OA Sources**

168 We conducted continuous measurements from 28 November to 28 December 2019, characterizing a winter period
169 with a mean PM₁ concentration of $27.8 \pm 15.3 \mu\text{g m}^{-3}$. This concentration is characterized as moderate; it closely
170 matches historical winter PM₁ means in Seoul (Kim et al., 2017) and implies an equivalent PM_{2.5} concentration is

171 about $34.8 \mu\text{gm}^{-3}$ (using a Korea-specific $\text{PM}_1/\text{PM}_{2.5} \approx 0.8$ (Kwon et al., 2023), which is near the national 24-h $\text{PM}_{2.5}$
172 standard ($35 \mu\text{gm}^{-3}$) (AirKorea). The full co-evolution of PM_1 , gaseous pollutants, and meteorological conditions
173 is provided in Fig. S6, showing an average ambient temperature of $1.76 \pm 4.3^\circ\text{C}$ and average relative humidity (RH)
174 of $56.9 \pm 17.5\%$ during the study.

175 Figure 1 summarizes the overall non-refractory submicron aerosol (NR- PM_1) composition and the identified OA
176 factors. Organics (41%) and nitrate (30%) were the most abundant chemical components of PM_1 , followed by
177 ammonium (12%), sulfate (10%), BC (5%), and chloride (3%) (Fig. 1a). Among the organic aerosols, six OA
178 factors were identified during the winter of 2019: hydrocarbon-like OA (HOA; 14%; O:C = 0.13), cooking-related
179 OA (COA; 21%; O:C = 0.18), nitrogen-enriched OA (NOA; 2%; O:C = 0.22), biomass burning OA (BBOA; 13%;
180 O:C = 0.25), and two types of secondary organic aerosols—less-oxidized oxygenated OA (LO-OOA; 30%; O:C =
181 0.68) and more-oxidized oxygenated OA (MO-OOA; 20%; O:C = 1.15) (Fig. 1e and Fig. S2). These compositions
182 are consistent with previous wintertime observations in Kim et al. (2017), with the exception of newly resolved
183 NOA source. In the following sections, we describe each OA factor in the order of secondary OA (SOA), primary
184 OA (POA) and finally introduce NOA, which—while related to combustion POA—emerged as a distinct, nitrogen-
185 rich factor under the winter conditions of this study.

186 PM_1 mass concentrations varied widely, ranging from 4.61 to $91.4 \mu\text{g m}^{-3}$, largely due to two severe haze episodes
187 that occurred between December 7–12 and December 22–26 (Fig. 1). During these episodes, average
188 concentrations increased significantly, driven primarily by elevated levels of nitrate and organic aerosols—
189 particularly MO-OOA and NOA (Fig. 1f,g). Back-trajectory clustering shows frequent short-range recirculation
190 over the Seoul Metropolitan Area during haze (Cluster 1; Fig. S8), and the time series indicates persistently low
191 surface wind speeds during these periods (1.73 ± 0.89 vs. 2.34 ± 1.18 (clean)) (Fig. S6). These patterns indicate
192 stagnation-driven accumulation of local emissions, consistent with the simultaneous increase of MO-OOA and
193 NOA that are examined in detail in subsequent sections. Such haze episodes, characterized by local emission
194 buildup and secondary aerosol production, are a typical wintertime feature, as also reported in Kim et al. (2017).

195 3.1.1 Secondary organic aerosols (SOA)

196 In this study, two OOA factors—more-oxidized OOA (MO-OOA) and less-oxidized OOA (LO-OOA)—were
197 identified, together accounting for approximately half of the total organic aerosol (OA) mass. This fraction is
198 notably higher than that reported in previous wintertime urban studies (Kim et al., 2017; Zhang et al., 2007). Both

199 OOAs exhibited characteristic mass spectral features, including prominent peaks at m/z 44 (CO_2^+) and m/z 43
200 ($\text{C}_2\text{H}_3\text{O}^+$), which are widely recognized as markers of oxygenated organics (Fig. S2e, S3f). The oxygen-to-carbon
201 (O:C) ratios for MO-OOA and LO-OOA were 1.15 and 0.68, respectively, indicating both factors are highly
202 oxidized relative to the primary OA factors (HOA, COA, BBOA) and that MO-OOA is substantially more oxidized
203 than LO-OOA. The O:C ratio of MO-OOA was especially elevated, exceeding those reported in previous Seoul
204 campaigns—0.68 in winter 2015 (Kim et al., 2017), 0.99 in spring 2019 (Kim et al., 2020), and 0.78 in fall 2019
205 (Jeon et al., 2023)—while the LO-OOA ratio was within a similar range.

206 MO-OOA showed strong correlations with secondary inorganic species such as nitrate ($r = 0.90$), ammonium ($r =$
207 0.92), and sulfate ($r = 0.81$), consistent with its formation through regional and local photochemical aging processes
208 (Fig. S3). In contrast, LO-OOA exhibited only modest correlations with sulfate, nitrate, and ammonium ($r = 0.50$,
209 0.51, and 0.42, respectively). This weaker coupling indicates that LO-OOA represents a less aged oxygenated OA
210 component (fresh SOA), distinguishable from the more aged, highly processed MO-OOA which tracks closely with
211 secondary inorganic species. Regarding potential primary influence, LO-OOA does not exhibit a pronounced m/z
212 60 (levoglucosan) signal (Figs. S2 and 9). While the levoglucosan marker (f_{60}) is known to diminish with
213 atmospheric aging and can become weak or undetectable downwind (Hennigan et al., 2010; Cubison et al., 2011),
214 the absence of a distinct peak combined with the separation from inorganic salts suggests that LO-OOA is best
215 characterized as freshly formed secondary organic aerosol likely originating from the rapid oxidation of local
216 anthropogenic precursors.

217 **3.1.2 Primary organic aerosols (POA)**

218 Three primary organic aerosol (POA) factors were identified in this study: hydrocarbon-like OA (HOA), cooking-
219 related OA (COA), and biomass burning OA (BBOA). These three components exhibited mass spectral and
220 temporal characteristics consistent with previous observations in Seoul and other urban environments. HOA was
221 characterized by dominant alkyl fragment ions ($\text{C}_n\text{H}_{2n+1}^+$ and $\text{C}_n\text{H}_{2n-1}^+$; Fig. S2a) and a low O:C ratio (0.13),
222 consistent with traffic-related emissions (0.05–0.25) (Canagaratna et al., 2015). It showed strong correlations with
223 vehicle-related ions C_3H_7^+ ($r = 0.79$) and C_4H_9^+ ($r = 0.86$) (Kim et al., 2017; Canagaratna et al., 2004; Zhang et al.,

224 2005), and exhibited a distinct morning rush hour peak (06:00–08:00), followed by a decrease likely driven by
225 boundary layer expansion (Fig. S3a).

226 COA, accounting for 21% of OA, showed higher contributions from oxygenated ions than HOA, with tracer peaks
227 at m/z 55, 84 and 98 (Fig. S2b) consistent with cooking emissions (Sun et al., 2011). COA showed an enhanced
228 signal at m/z 55 relative to m/z 57, with a 55/57 ratio of 3.11, substantially larger than that of HOA (1.10). This
229 elevated ratio is consistent with previously reported AMS COA spectra in urban environments (e.g., Allan et al.,
230 2010; Mohr et al., 2012; Sun et al., 2011), supporting our factor assignment. It correlated strongly with cooking-
231 related ions such as $\text{C}_3\text{H}_3\text{O}^+$ ($r = 0.94$), $\text{C}_5\text{H}_8\text{O}^+$ ($r = 0.96$), and $\text{C}_6\text{H}_{10}\text{O}^+$ ($r = 0.98$) (Fig. S3h), and displayed
232 prominent peaks during lunch and dinner hours, reflecting typical cooking activity patterns.

233 BBOA was identified based on characteristic ions at m/z 60 ($\text{C}_2\text{H}_4\text{O}_2^+$) and 73 ($\text{C}_3\text{H}_5\text{O}^+$), both of which are
234 associated with levoglucosan—a well-established tracer for biomass burning (Simoneit et al., 2002). Its relatively
235 high f_{60} and low f_{44} values (Fig. S9) indicate that the BBOA observed in this study was relatively fresh and had not
236 undergone extensive atmospheric aging (Cubison et al., 2011). Regarding source location, several pathways can
237 influence Seoul’s biomass burning signature. First, urban/peri-urban small-scale burning (e.g., solid-fuel use in
238 select households, restaurant charcoal use, and intermittent waste burning) has been reported and can enhance
239 BBOA locally (Kim et al., 2017). Second, nearby agricultural-residue burning in surrounding provinces occurs
240 seasonally and can episodically impact the metropolitan area (Han et al., 2022). Third, regional transport from
241 upwind regions (e.g., northeastern China/North Korea) can bring biomass burning influenced air masses under
242 northerly/northwesterly flow (Lamb et al., 2018; Nault et al., 2018). In this dataset, the nighttime and early-
243 morning enhancements and trajectory clusters showing regional recirculation indicate a predominantly local/near-
244 source contribution during the study period, with episodic non-local influences remaining possible (Fig. S8).

245 3.1.2.1 Nitrogen-containing organic aerosol (NOA)

246 A distinct nitrogen-containing organic aerosol (NOA) factor was resolved in this study, whereas earlier wintertime
247 AMS–PMF analyses in Seoul did not isolate such a component. The NOA factor exhibited the highest nitrogen-to-
248 carbon (N:C) ratio (0.22) and the lowest oxygen-to-carbon (O:C) ratio (0.19) among all POA factors (Fig. S2),
249 indicating a chemically reduced, nitrogen-rich composition. The NOA mass spectrum was dominated by amine-
250 related fragments including m/z 30 (CH_4N^+), 44 ($\text{C}_2\text{H}_6\text{N}^+$), 58 ($\text{C}_3\text{H}_8\text{N}^+$), and 86 ($\text{C}_5\text{H}_{12}\text{N}^+$) (Fig. 3a). The spectral
251 signature of the factor is defined by the characteristic dominance of the m/z 44 fragment, which typically serves as

252 the primary marker for dimethylamine (DMA)-related species, closely followed by m/z 58 (trimethylamine, TMA)
253 and m/z 30 (methylamine, MA). This profile is in strong agreement with NOA factors resolved via PMF in other
254 polluted environments. For instance, the dominance of m/z 44 and m/z 30 aligns with amine factors reported in
255 New York City (Sun et al., 2011) and Pasadena, California (Hayes et al., 2013). This DMA-dominated signature is
256 also consistent with seasonal characterization of organic nitrogen in Beijing (Xu et al., 2017) and Po Valley, Italy
257 (Saarikoski et al., 2012), reinforcing the common chemical signature of reduced organic nitrogen across diverse
258 urban and regional environments.

259 In this study, NOA contributed approximately 2 % of total OA, comparable to urban contributions reported in
260 Guangzhou (3 %; Chen et al., 2021), Pasadena (5 %; Hayes et al., 2013), and New York (5.8 %; Sun et al., 2011).
261 These similarities suggest that the NOA factor observed in Seoul reflects a broader class of urban wintertime
262 reduced-nitrogen aerosols rather than a site-specific anomaly. Furthermore, the presence of non-negligible signals
263 at m/z 58 and m/z 86 supports the contribution of slightly larger alkylamines, a pattern that aligns well with
264 established AMS laboratory reference spectra (Ge et al., 2011; Silva et al., 2008). In most urban environments, the
265 detectability of NOA appears to depend strongly on the interplay between emission strength, stagnation, and
266 humidity—which together govern the particle-phase partitioning of volatile amines.

267 These amines are commonly emitted during the combustion of nitrogen-rich biomass and proteinaceous materials
268 and are frequently associated with biomass-burning emissions (Ge et al., 2011). Previous molecular analyses in
269 Seoul also indicate DMA, MA, and TMA as the dominant amine species in December (Baek et al., 2022). While
270 other amines such as triethylamine (TEA), diethylamine (DEA), and ethylamine (EA) may contribute via
271 industrial/solvent pathways (e.g., chemical manufacturing, petrochemical corridors, wastewater treatment), our
272 HR-AMS spectra are dominated by small alkylamine fragments (m/z 30, 44, 58, 86) and the diurnal behavior co-
273 varies with combustion markers (Fig. 2), indicating a primarily combustion-linked influence. Nevertheless, recent
274 urban measurements and sector-based analyses show that industrial activities can contribute measurable amines in
275 cities (Tiszenkel et al., 2024; Zheng et al., 2015; Mao et al., 2018; Shen et al., 2017; Yao et al., 2016). Accordingly,
276 a minor NOA contribution from solvent/industrial amines cannot be excluded. NOA exhibited a nighttime–early-
277 morning enhancement (Fig. 2a), similar to BBOA, indicating that both factors are influenced by wintertime
278 combustion and residential heating, which are known sources of small alkylamines and amides (You et al., 2014;
279 Yao et al., 2016). Strong correlations of NOA with CH_4N^+ ($r = 0.95$) and $\text{C}_2\text{H}_6\text{N}^+$ ($r = 0.91$) (Fig. 2) further support
280 the presence of reduced-nitrogen species associated with these combustion activities. However, the time series of

281 NOA and BBOA are not strongly correlated (Fig. 2 and Fig. S7). This contrast reflects their differing behaviors:
282 BBOA follows a relatively regular daily emission pattern, whereas NOA appears predominantly during stagnant
283 haze periods (Fig. 1) when cold, humid, and low-wind conditions allow semi-volatile amines to partition to the
284 particle phase and form low-volatility aminium salts. Thus, NOA in wintertime Seoul likely reflects a combination
285 of shared primary combustion influences and enhanced secondary processing of amine-containing precursors under
286 meteorological conditions that favor partitioning and accumulation.

287 Detection of particulate NOA using real time measurement has been challenging due to its low concentration and
288 high volatility. Although Baek et al. (2022) identified nitrogen-containing species in Seoul via year-round filter-
289 based molecular analysis, PMF-based resolution of NOA in real time has not been previously reported. The
290 successful identification in this study is likely attributable to favorable winter meteorological conditions—
291 specifically low temperatures (-0.24°C) and persistently high relative humidity ($\sim 57\%$) compared to the 2017
292 winter season (Kim et al., 2017)—that enhanced gas-to-particle partitioning of semi-volatile amines, thereby
293 enabling their detection (Fig. S2). NOA concentrations frequently exceeded $1 \mu\text{g m}^{-3}$ when RH surpassed 60% (Fig.
294 2), supporting the importance of RH-driven partitioning and the subsequent formation of low-volatility aminium
295 salts (Rovelli et al., 2017). Although extremely low temperatures may inhibit NOA formation due to the transition
296 of aerosol particles into solid phase (Ge et al., 2011; Srivastava et al., 2022), the combination of consistently cold
297 and humid conditions during the measurement period likely promoted the partitioning of semi-volatile amines into
298 the particle phase. In addition, episodic haze events further elevated NOA levels, increasing its contribution to OA
299 from 1% during clean periods to as much as 3% (Fig. 1f–h). These high-concentration events likely improved the
300 signal-to-noise ratio, facilitating PMF resolution. Back-trajectory clustering indicates that NOA-enhanced events
301 were dominated by short-range recirculation (Cluster 1; Fig. S7), consistent with the short atmospheric lifetimes
302 and high reactivity of alkylamines (Nielsen et al., 2012; Hanson et al., 2014). Overall, the factor reflects semi-
303 volatile, reduced-nitrogen species originating from primary urban combustion sources, with their observed particle-
304 phase mass amplified by rapid secondary partitioning and salt formation under seasonally favorable conditions.
305

306 3.2 Volatility of Non-Refractory Species

307 Figure 4 presents thermograms of non-refractory (NR) species measured by HR-ToF-AMS. The mass fraction
308 remaining (MFR) after thermodenuder (TD) treatment follows the typical volatility trend reported in previous
309 studies (Xu et al., 2016; Kang et al., 2022; Jeon et al., 2023; Huffman et al., 2009): nitrate was the most volatile,

310 followed by chloride, ammonium, organics, and sulfate. Nitrate showed the steepest decline with increasing
311 temperature, with a T_{50} of ~ 67 °C—substantially higher than that of pure ammonium nitrate (~ 37 °C; Huffman et
312 al., 2009). At 200 °C, $\sim 2\%$ of the initial nitrate signal remained (Fig. 4). Since pure ammonium nitrate fully
313 evaporates well below this temperature (Huffman et al., 2009), this small residual fraction likely represents the
314 least volatile portion of organic nitrates. Compared to previously reported fall conditions ($T_{50} \sim 73$ °C, incomplete
315 evaporation), winter nitrate appeared more volatile, indicating relatively fewer non-volatile nitrate forms (e.g.,
316 Kang et al., 2022; Jeon et al., 2023). Sulfate exhibited the highest thermal stability among the measured species.
317 The thermogram showed a relatively stable mass fraction (MFR > 0.8) up to ~ 130 °C, followed by a sharp decline
318 at temperatures above 140 °C (Fig. 4). This profile is consistent with the typical volatilization behavior of
319 ammonium sulfate in TD-AMS, which requires higher temperatures to evaporate compared to nitrate or organics
320 (Huffman et al., 2009). At 200 °C, approximately 25% of the sulfate mass remained. This residual suggests the
321 presence of a sulfate fraction with lower volatility than pure ammonium sulfate, likely associated with
322 organosulfates or low-volatility mixtures, whereas refractory metal sulfates are not efficiently detected by the AMS
323 (Canagaratna et al., 2007). Ammonium showed intermediate volatility, with T_{50} between nitrate and sulfate. Its
324 slightly lower winter T_{50} suggests stronger nitrate association. Residual ammonium at 200 °C was consistent ($\sim 4\%$)
325 in previously reported spring/fall measurements (Kang et al., 2022; Jeon et al., 2023). Chloride volatility was
326 broadly consistent with prior AMS studies, with T_{50} values comparable across seasons (e.g., Xu et al., 2016; Jeon
327 et al., 2023). The near-complete evaporation observed in winter ($\sim 4\%$ residual at 200 °C, Fig. 4) indicates that the
328 chloride measured here was dominated by volatile inorganic chloride, specifically ammonium chloride (NH_4Cl),
329 which fully evaporates at relatively low temperatures (Huffman et al., 2009). By contrast, metal chlorides (e.g.,
330 NaCl , KCl) are refractory and far less volatile; they are also poorly detected by the AMS (Canagaratna et al., 2007).
331 The lower residual in winter compared to fall ($\sim 10\%$) therefore suggests that wintertime chloride consisted almost
332 exclusively of pure ammonium chloride, whereas the fall samples may have contained a minor fraction of less
333 volatile or refractory chloride species. Organics exhibited moderate volatility ($T_{50} \sim 120$ °C), and their thermogram
334 showed a gradual, continuous decrease in mass fraction with increasing TD temperature. This smooth profile
335 reflects the presence of a broad distribution of organic compounds spanning SVOC to LVOC ranges, in contrast to
336 inorganic species such as nitrate or ammonium chloride, which often show more abrupt losses at characteristic
337 temperatures (Huffman et al., 2009; Xu et al., 2016). This behavior is consistent with previous TD-AMS
338 observations in Seoul during spring and fall (Kang et al., 2022; Jeon et al., 2023).

339 **3.2.1 Volatility Profiles of Organic sources**

340 Figure 5 presents the volatility distributions of six OA sources within the volatility basis set (VBS) framework.
341 Volatility is expressed as the effective saturation concentration (C^* , $\mu\text{g m}^{-3}$), where higher C^* values correspond
342 to higher volatility. Following Donahue et al. (2009), C^* values are categorized into four bins: extremely low-
343 volatility organic compounds (ELVOCs, $\log C^* < -4.5$), low-volatility organic compounds (LVOCs, $-4.5 < \log$
344 $C^* < -0.5$), semi-volatile organic compounds (SVOCs, $-0.5 < \log C^* < 2.5$), and intermediate-volatility organic
345 compounds (IVOCs, $2.5 < \log C^* < 6.5$).

346 Among the primary OA (POA) sources, hydrocarbon-like OA (HOA) exhibited the highest volatility, with mass
347 predominantly distributed in the SVOC and IVOC ranges, consistent with its chemically reduced nature ($\text{O:C} =$
348 0.13) and direct combustion origin. Mass fraction remaining (MFR) results (Fig. S9) further support this, showing
349 rapid mass loss at lower temperatures. Biomass burning OA (BBOA) and nitrogen-containing OA (NOA) also
350 showed high volatility, peaking in the SVOC–IVOC range ($\log C^* = 1–3$), but displayed slightly higher O:C ratios
351 (0.25 and 0.19, respectively). This modest enhancement in O:C reflects their source composition—biomass
352 combustion produces partially oxygenated organic species (e.g., levoglucosan, phenols), and NOA contains
353 nitrogen-bearing functional groups—rather than enhanced atmospheric oxidation. Cooking-related OA (COA)
354 showed a more moderate volatility profile, with mass more evenly distributed across the LVOC and SVOC bins.
355 This behavior differs from that of BBOA, which is slightly more oxidized yet more volatile. This apparent
356 decoupling between oxidation state and volatility is a characteristic feature of COA reported in previous volatility
357 studies (Paciga et al., 2016; Kang et al., 2022). These studies attribute the lower volatility of COA to its abundance
358 of high-molecular-weight fatty acids (e.g., oleic, palmitic, and stearic acids) and glycerides (Mohr et al., 2009; He
359 et al., 2010). Unlike the smaller, fragmented molecules typical of biomass burning, these lipid-like compounds
360 possess high molar masses that suppress volatility, even though their long alkyl chains result in low O:C ratios.

361 For secondary OA (SOA), less-oxidized oxygenated OA (LO-OOA) exhibited the lowest volatility, with substantial
362 mass in the LVOC and ELVOC bins ($C^* \approx 10^{-3}–10^{-4}$). This is in agreement with previous findings in Seoul during
363 spring (Kang et al., 2022). In contrast, more-oxidized OOA (MO-OOA), despite its higher oxidation state ($\text{O:C} =$

364 1.15), displayed greater volatility, with a peak at $C^* \approx 10^1$. This discrepancy likely reflects differences in formation
365 and aging processes, as discussed further in Section 3.3.

366 Overall, the volatility characteristics across OA factors suggest that oxidation state alone does not fully explain
367 volatility. Rather, volatility is shaped by a combination of emission source, emission timing, temperature, and
368 atmospheric processing. These findings highlight the importance of integrating both chemical and physical
369 characterization to better understand OA formation and aging across seasons.

370 **3.3 Aging effect on volatility from 2D VBS**

371 Generally, the oxygen-to-carbon (O:C) ratio of organic aerosols (OA) is inversely related to their volatility. As O:C
372 increases through aging, the effective saturation concentration (C^*) typically decreases, resulting in lower volatility
373 (Donahue et al., 2006; Jimenez et al., 2009). This relationship arises because oxidative functionalization introduces
374 polar groups (e.g., hydroxyl, carboxyl) that increase molecular weight and enhance intermolecular hydrogen
375 bonding, thereby reducing the effective saturation concentration (C^*) and promoting particle-phase retention
376 (Jimenez et al., 2009; Kroll and Seinfeld, 2008; Donahue et al., 2011). However, in this study, the most oxidized
377 OA factor—MO-OOA, with a high O:C ratio of 1.15—exhibited unexpectedly high volatility. Its volatility
378 distribution was skewed toward SVOCs and IVOCs (Fig. 5), and its rapid mass loss in MFR thermograms (Fig.
379 S9) further indicated low thermal stability. This observation appears to contradict the usual inverse O:C–volatility
380 relationship; however, under winter haze conditions—with suppressed O_3 /low OH, particle-phase autoxidation and
381 fragmentation can yield higher-O:C yet more volatile products, with enhanced condensation on abundant particle
382 surface area (details below).

383 Viewed against prior TD-AMS results, the volatility of Seoul’s winter MO-OOA presents a unique case,
384 particularly in the nature of its O:C-volatility relationship. Prior urban studies have commonly reported substantial
385 SVOC-OA, consistent with high photochemical activity or elevated loadings; for example, prior TD-AMS studies
386 in Mexico City, Los Angeles, Beijing, and Shenzhen have all reported substantial SVOC–IVOC contributions
387 during polluted periods, indicating that high OA volatility is a common feature of urban environments across
388 seasons (Cappa and Jimenez, 2010; Xu et al., 2019; Cao et al., 2018). While these comparisons establish that
389 volatile OA is common, they generally did not report the factor-level inversion observed here, where the highly-
390 oxidized OOA component (MO-OOA) was more volatile than a less-oxidized OOA (LO-OOA). This behavior is
391 distinct from findings in colder, lower-loading regimes; wintertime Paris, for instance, maintained the conventional

392 hierarchy where the more-oxidized OOA was comparatively less volatile (Paciga et al., 2016). Furthermore,
393 seasonal context within Seoul showed springtime OA with lower oxidation levels than our winter MO-OOA despite
394 similar SVOC contributions (Kang et al., 2022). This comprehensive comparison underscores the unusual nature
395 of the O:C-volatility relationship observed under the specific winter haze conditions in Seoul.

396

397 **3.3.1 High-volatility nature of MO-OOA in Seoul wintertime**

398 MO-OOA exhibited high O:C ratios and high apparent volatility, characteristics that were further amplified during
399 haze episodes—periods marked by reduced ozone levels, low solar radiation, and elevated aerosol mass
400 concentrations (Fig. 7 and Fig. S6, yellow shading). Spectrally, MO-OOA was defined by a consistently high f_{44}
401 (CO_2^+) signal and a comparatively stable f_{43} ($\text{C}_2\text{H}_3\text{O}^+$) signal relative to LO-OOA (Fig. 6). Notably, when MO-
402 OOA concentrations intensified during haze, only f_{44} was significantly enhanced, while f_{43} remained nearly
403 unchanged (Fig. 6). This trend is corroborated by the haze–non-haze comparison (Fig. S12), where haze periods
404 (including high MO-OOA intervals) showed elevated contributions from oxygenated fragments (m/z 28, 29, 44)
405 and higher O:C ratios. In contrast, non-haze periods were characterized by larger fractional contributions from
406 hydrocarbon-like fragments (m/z 41, 43, 55, 57). The observed temporal pattern—elevated f_{44} without
407 corresponding changes in f_{43} —is a typical signature of highly oxidized and fragmented organic aerosol (Figs. 6 and
408 7), suggesting that aging was dominated by fragmentation rather than functionalization (Kroll et al., 2009). These
409 spectral patterns collectively indicate that MO-OOA is highly oxidized yet remains relatively volatile compared to
410 LO-OOA.

411 The elevated volatility of MO-OOA despite its high O:C (~1.15) indicates that oxidation under these haze
412 conditions did not follow the classical multi-generational OH-driven aging pathway, which typically increases
413 molecular mass and reduces volatility. Instead, the data align with fragmentation-dominated aging, where highly
414 oxygenated but lower-molecular-weight compounds (e.g., small acids or diacids) are formed. Prior field and
415 laboratory studies using online AMS/FIGAERO-CIMS and EESI-TOF have similarly reported high-O:C yet
416 volatile product distributions characterized by high f_{44} and stable f_{43} (Kroll et al., 2009; Ng et al., 2010; Chhabra et
417 al., 2011; Lambe et al., 2012; Lopez-Hilfiker et al., 2016; D’Ambro et al., 2017).

418 While direct mechanistic measurements were not available in this study, we hypothesize that the formation of this
419 volatile, high-O:C component may be driven by specific low-light oxidation pathways consistent with the observed
420 environmental conditions. The suppressed ozone levels during haze likely indicate a low-OH oxidation regime

421 (Fig. 7). Under such conditions, radical chemistry involving NO_3 (which is longer-lived in low light) or particle-
422 phase autoxidation could preferentially produce highly oxygenated but relatively small organic fragments (Ehn et
423 al., 2014; Zhao et al., 2023). Although haze suppresses photolysis, HONO concentrations—maintained via
424 heterogeneous conversion or surface emissions—could still provide a non-negligible source of OH (Gil et al., 2021;
425 Kim et al., 2024; Slater et al., 2020). Furthermore, the high aerosol mass loadings during haze (C_{oa}) provide
426 abundant surface area for absorptive partitioning (Pankow, 1994; Donahue et al., 2006). This increased partitioning
427 mass allows even relatively volatile, oxidized compounds to condense into the particle phase, contributing to the
428 high apparent volatility and oxidation state observed (Jimenez et al., 2009; Ng et al., 2016). Consequently, these
429 results underscore the need for SOA models to incorporate fragmentation-dominated pathways to accurately
430 represent wintertime haze evolution.

431 **4 Conclusions**

432 This study provides a comprehensive characterization of wintertime submicron aerosols (PM_1) in Seoul, integrating
433 chemical composition, volatility measurements, and source apportionment to reveal critical insights into urban OA
434 evolution. The two most significant findings are the robust real-time identification of a nitrogen-containing organic
435 aerosol (NOA) factor and the observation of unexpected volatility behavior in highly oxidized OA. The NOA
436 factor, spectrally dominated by low-molecular-weight alkylamine fragments, was successfully resolved primarily
437 due to the accumulation of pollutants during wintertime stagnation, which sufficiently enhanced the spectral signals
438 of these semi-volatile species for identification. Its temporal and chemical characteristics point to a mixed
439 primary/secondary origin: driven by direct combustion emissions (e.g., residential heating) but significantly
440 enhanced by the rapid gas-to-particle partitioning of semi-volatile amines under cold, humid conditions.
441 Concurrently, the volatility analysis revealed a notable decoupling between oxidation state and volatility for the
442 More-Oxidized Oxygenated OA (MO-OOA). Despite its high O:C ratio (~1.15), MO-OOA exhibited elevated
443 volatility, a deviation from classical aging models that typically associate high oxidation with low volatility. This
444 behavior is attributed to the specific conditions of winter haze—reduced photolysis and high aerosol mass
445 loadings—which favor fragmentation-dominated aging pathways and the absorptive partitioning of volatile
446 oxygenated products.

447 These results revise our understanding of wintertime aerosol dynamics and underscore the limitations of current
448 models in representing reduced-nitrogen species and non-canonical oxidation pathways. To address the remaining

449 uncertainties, future research should prioritize evaluating the seasonal variability of NOA to better disentangle the
450 influence of meteorological drivers from specific emission sources. Concurrently, there is a critical need to directly
451 probe radical oxidation mechanisms, such as RO_2 autoxidation and NO_3 chemistry, particularly under haze
452 conditions. Integrating these field inquiries with laboratory studies and advanced molecular-level measurements
453 (e.g., FIGAERO-CIMS, EESI-TOF) will be essential for constraining the formation, lifetime, and climate impacts
454 of these complex organic aerosol components in polluted megacities.

455 **Data availability.**

456 Data presented in this article are available upon request to the corresponding author.

457 **Acknowledgements**

458 This work was supported by the National Research Foundation of Korea (NRF) grant funded by the Korea
459 government (MSIT) (RS-2025-00514570), the project “development of SMaRT based aerosol measurement and
460 analysis systems for the evaluation of climate change and health risk assessment” operated by Seoul National
461 University (900-20240101). Also this research was supported by Particulate Matter Management Specialized Graduate
462 Program through the Korea Environmental Industry & Technology Institute (KEITI) funded by the Ministry of Environment
463 (MOE).

464 **Author Contributions**

465 HK designed the study and prepared the manuscript. JJ operated the TD-AMS and analyzed the TD-AMS data. JM
466 curated and managed the dataset. HGK conducted the volatility analysis of organic aerosol (OA)

467

468 **Competing interests.**

469 The authors declare that they have no conflict of interest.

470

471

472

473

474

475

476

477

478

479

480

481

482

483

484

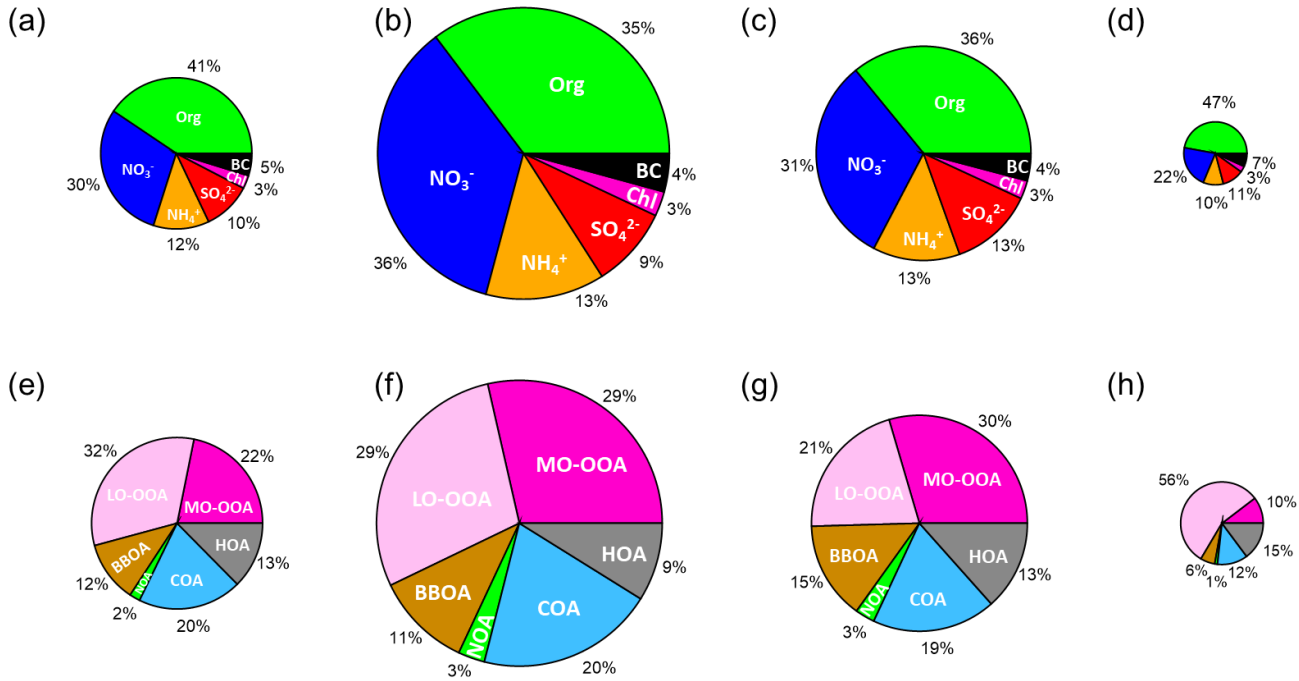
485

486 Tables and Figures

487

488

489

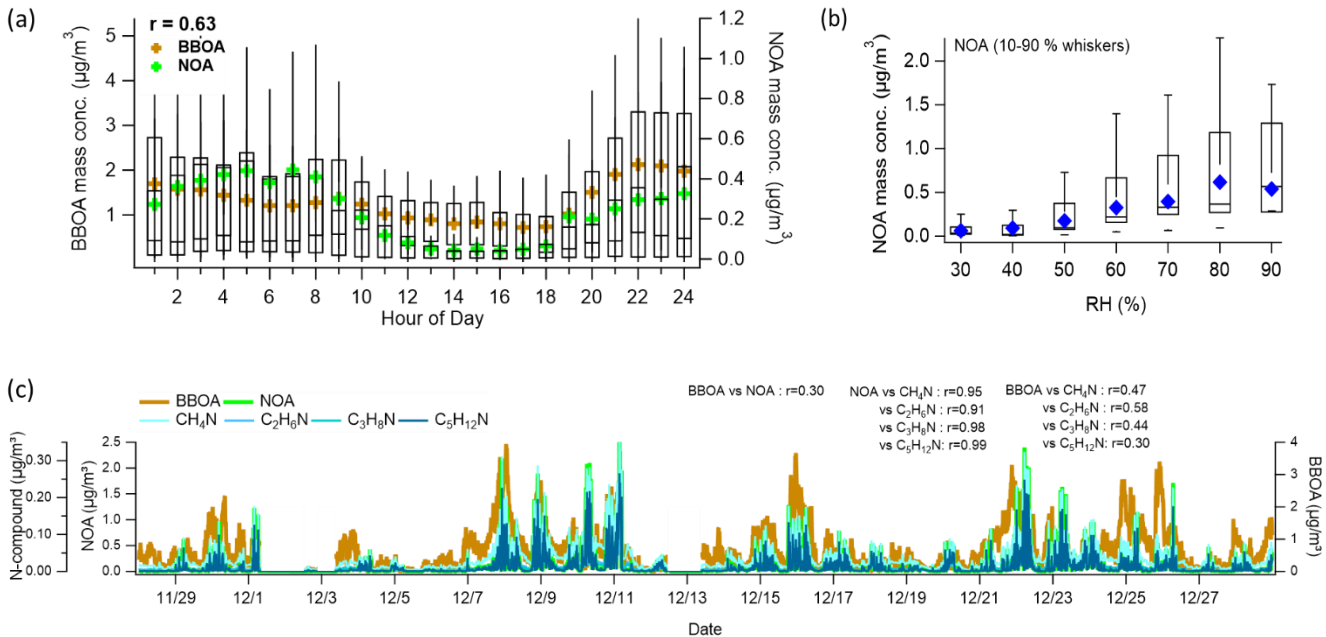


490

	Period	Standard	Avg. Mass conc. ($\mu\text{g m}^{-3}$)
Total	2019.11.28 ~ 2019.12.28		Avg $\text{PM}_1 = 26.37$
Clean	2019.12.04 ~ 2019.12.06	Daily $\text{PM}_1 < 10.00 \mu\text{g m}^{-3}$	Avg $\text{PM}_1 = 9.98$
Haze 1	2019.12.07 ~ 2019.12.11	Daily $\text{PM}_1 > 30.00 \mu\text{g m}^{-3}$	Avg $\text{PM}_1 = 51.88$
Haze 2	2019.12.21 ~ 2019.12.25	Daily $\text{PM}_1 > 30.00 \mu\text{g m}^{-3}$	Avg $\text{PM}_1 = 37.71$

491

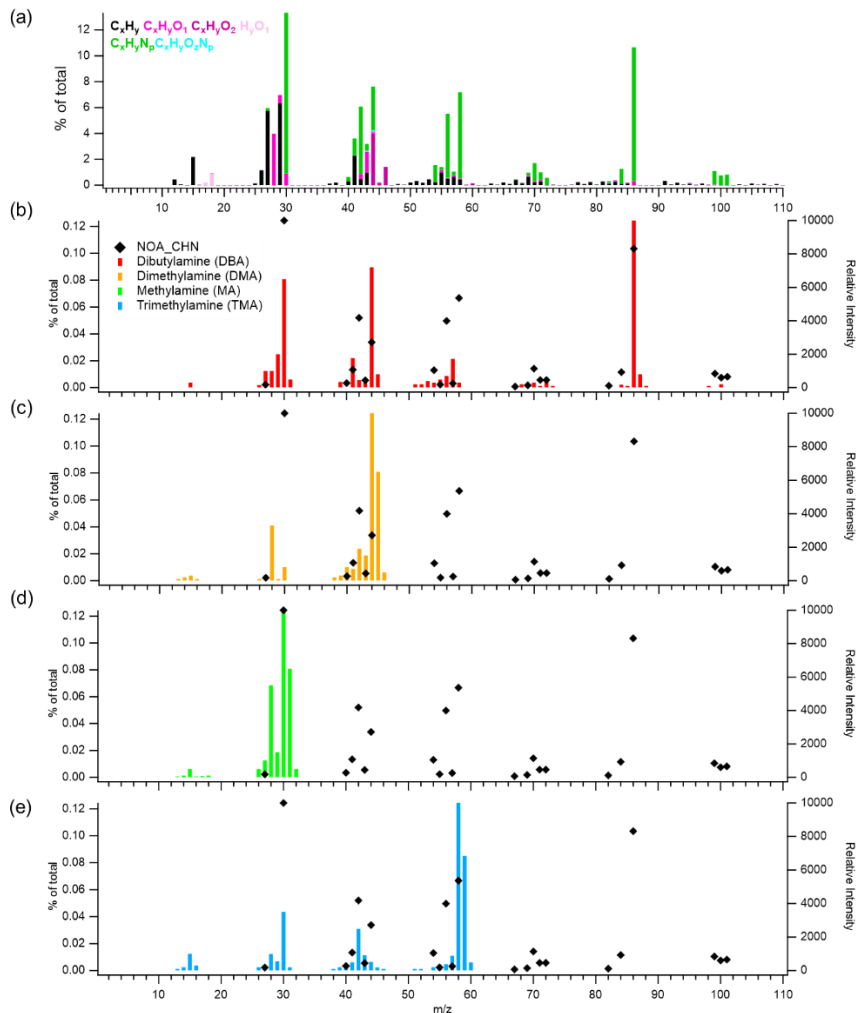
492 **Figure 1.** Compositional pie charts of PM_1 species for (a) the entire study period, (b) haze period 1, (c) haze period 2, and
 493 (d) a clean period; and of each OA source for (e) the entire study period, (f) haze period 1, (g) haze period 2, and (h) the
 494 clean period. Table. Standard and average PM_1 mass concentrations during the entire study period, haze period 1, haze period
 495 2, and the clean period.



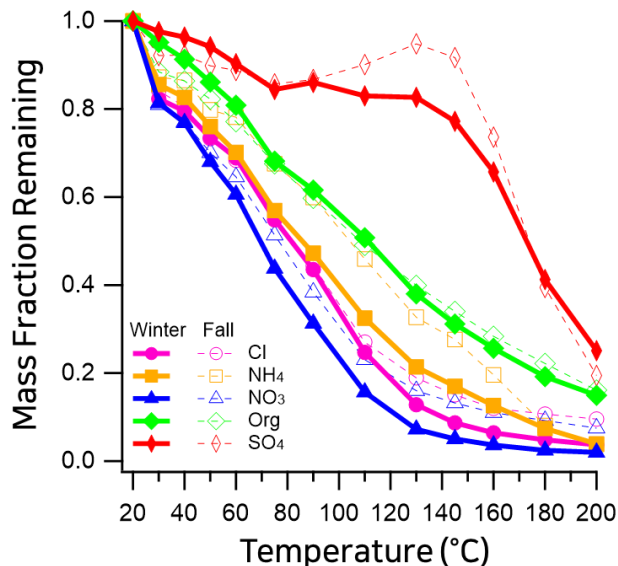
496

497

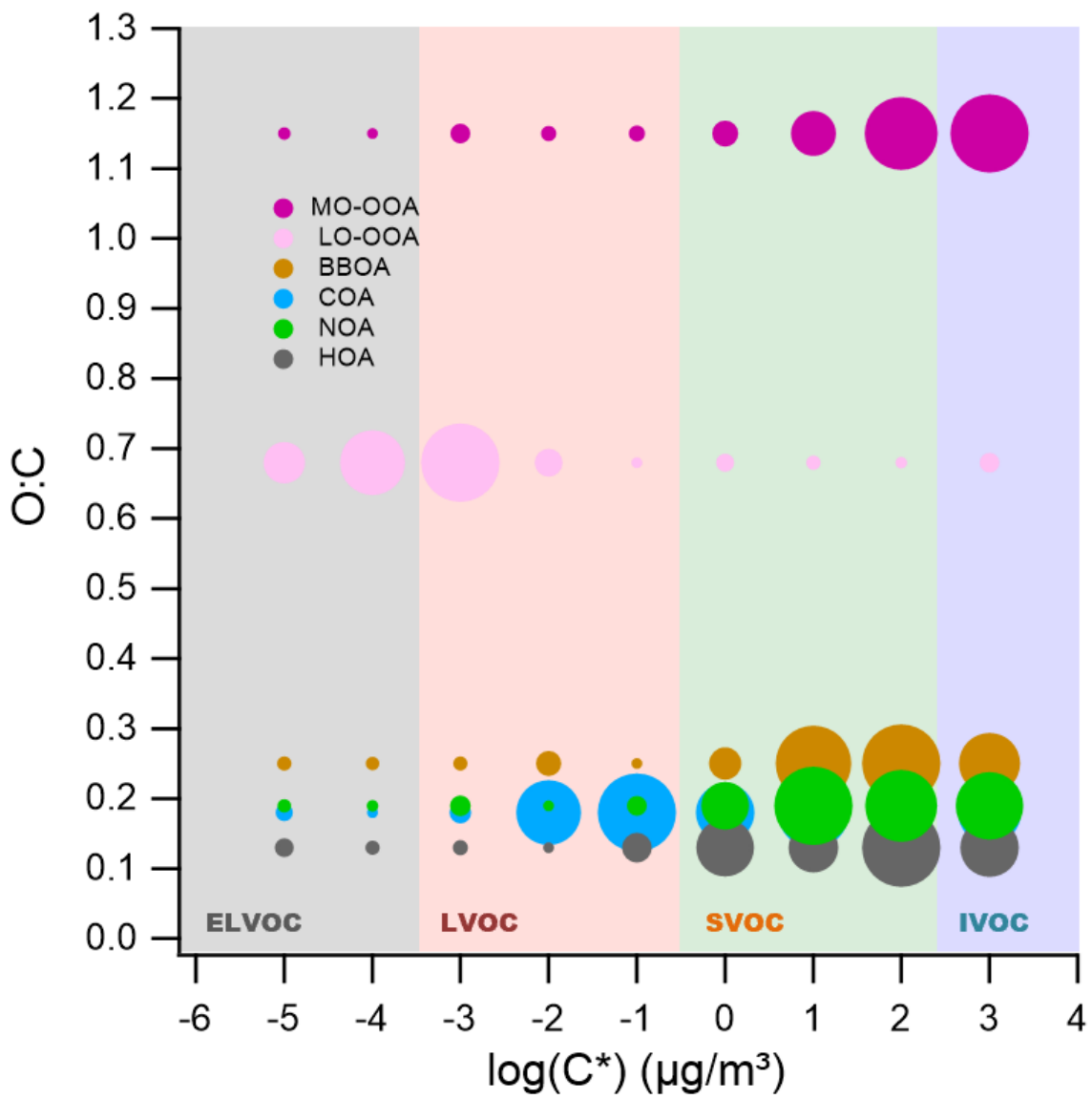
498 **Figure 2.** (a) Diurnal mean profiles of NOA and BBOA. Whiskers denote the 90th and 10th percentiles; box
 499 edges represent the 75th and 25th percentiles; the horizontal line indicates the median, and the colored marker
 500 shows the mean. The diurnal correlation between NOA and BBOA mean values is 0.63.
 501 (b) Relative humidity (RH)-binned nighttime (19:00–05:00) profile of NOA. Box and whisker definitions are the
 502 same as in panel (a). (c) Time series of NOA, BBOA, and amine-related ions (CH₄N⁺, C₂H₆N⁺, C₃H₈N⁺,
 503 C₅H₁₂N⁺), along with their correlations with NOA and BBOA.



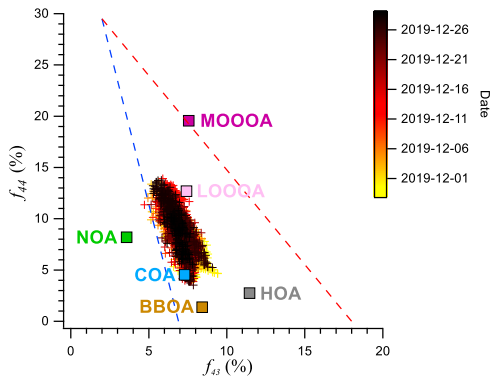
504
505 **Figure 3.** Mass spectra of (a) the NOA factor resolved by PMF analysis in this study, and reference spectra of amines from
506 the NIST library: (b) dibutylamine (DBA), (c) dimethylamine (DMA), (d) methylamine (MA), and (e) trimethylamine
507 (TMA). In panels (b)–(e), the left y-axis indicates the contribution of CHN-containing ions in the NOA factor (% of total),
508 while the right y-axis shows the relative intensity of each compound's mass spectrum from the NIST library.



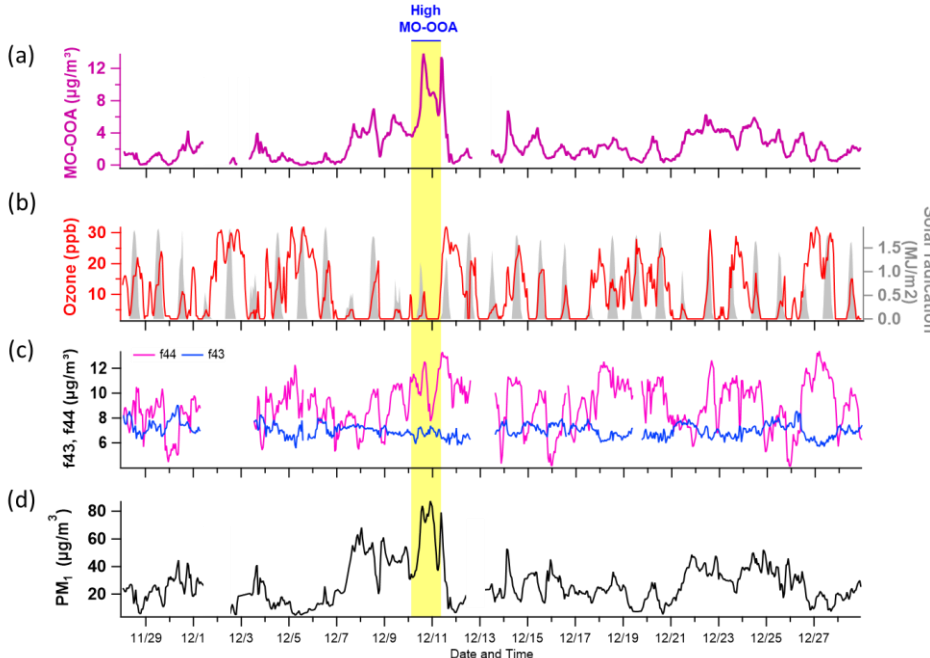
509 **Figure 4.** Mass fraction remaining (MFR) of non-refractory (NR) aerosol species measured in Seoul using a thermodenuder
 510 coupled to a high-resolution time-of-flight aerosol mass spectrometer (HR-ToF-AMS). Winter 2019 (this study; dashed) is
 511 compared with fall 2019 (previously reported; solid) (Jeon et al., 2023). Species include organics (magenta), nitrate (blue),
 512 sulfate (orange), ammonium (green), and chloride (red).



513
 514 **Figure 5.** Two-dimensional volatility basis set (2D-VBS) representation of organic aerosol (OA) sources identified in winter
 515 2019 in Seoul. The plot illustrates the relationship between the oxygen-to-carbon (O:C) ratio and the effective saturation
 516 concentration (C^*) for each OA source resolved via positive matrix factorization (PMF). Solid circles represent the volatility
 517 distribution across C^* bins, with marker size proportional to the mass fraction within each bin for the given source. Shaded
 518 regions correspond to different volatility classes: extremely low-volatility organic compounds (ELVOCs), low-volatility
 519 organic compounds (LVOCs), semi-volatile organic compounds (SVOCs), and intermediate-volatility organic compounds
 520 (IVOCs), delineated by their C^* values.



521 **Figure 6.** scatterplot of f_{44} (CO_2^+) versus f_{43} ($\text{C}_2\text{H}_3\text{O}^+$). for the measured organic aerosol. The data points are color-coded by
522 date to illustrate the temporal variation in OA composition throughout the observation period. The separated OA factors
523 (HOA, COA, BBOA, NOA, LO-OOA, and MO-OOA) are also shown to enable comparison of source contributions and
524 oxidation characteristics. The dashed line represents the typical f_{60} threshold associated with biomass-burning influence,
525 while the triangular boundary indicates the conventional oxidative aging trend in the f_{44} - f_{60} space.
526



527
528 **Figure 7.** Time series plots of (a) MO-OOA concentration, (b) ozone (O_3) and solar radiation, (c) f_{44} and f_{43} (indicative of
529 oxidation state), and (d) total PM_1 concentration. The period characterized by elevated MO-OOA levels is highlighted in bright
530 yellow. Panels (e)–(f) present comparative distributions of these variables—MO-OOA, O_3 and solar radiation, f_{44} and f_{43} , and
531 PM_1 —between the high MO-OOA period (shaded in blue) and the entire measurement period (indicated by gray hatching).
532

533 **References**

534 Allan, J. D., Alfarra, M. R., Bower, K. N., Williams, P. I., Gallagher, M. W., Jimenez, J. L., McDonald, A. G.,
535 Nemitz, E., Canagaratna, M. R., and Coe, H.: Quantitative sampling using an Aerodyne aerosol mass
536 spectrometer—2. Measurements of fine particulate chemical composition in two U.K. cities, *J. Geophys. Res.-*
537 *Atmos.*, 108, 4091, <https://doi.org/10.1029/2002JD002359>, 2003.

538 Allan, J. D., Williams, P. I., Morgan, W. T., Martin, C. L., Flynn, M. J., Lee, J., Nemitz, E., Phillips, G. J.,
539 Gallagher, M. W., and Coe, H.: Contributions from transport, solid fuel burning and cooking to primary organic
540 aerosols in two UK cities, *Atmos. Chem. Phys.*, 10, 647–668, <https://doi.org/10.5194/acp-10-647-2010>, 2010.

541 Baek, K. M., Park, E. H., Kang, H., Ji, M. J., Park, H. M., Heo, J., and Kim, H.: Seasonal characteristics of
542 atmospheric water-soluble organic nitrogen in PM2.5 in Seoul, Korea: Source and atmospheric processes of
543 free amino acids and aliphatic amines, *Sci. Total Environ.*, 807, 150785,
544 <https://doi.org/10.1016/j.scitotenv.2021.152335>, 2022.

545 Berndt, T., Richters, S., Jokinen, T., Hyttinen, N., Kurtén, T., Otkjær, R. V., Kjaergaard, H. G., Stratmann, F.,
546 Herrmann, H., Sipilä, M., Kulmala, M., and Ehn, M.: Hydroxyl radical-induced formation of highly oxidized
547 organic compounds, *Nat. Commun.*, 7, 13677, <https://doi.org/10.1038/ncomms13677>, 2016.

548 Bianchi, F., Kurtén, T., Riva, M., Mohr, C., Rissanen, M. P., Roldin, P., Berndt, T., Crounse, J. D., Wennberg, P.
549 O., Mentel, T. F., Wildt, J., Junninen, H., Jokinen, T., Kulmala, M., Worsnop, D. R., Thornton, J. A., Donahue,
550 N. M., Kjaergaard, H. G., and Ehn, M.: Highly oxygenated organic molecules (HOM) from gas-phase
551 autoxidation involving peroxy radicals: A key contributor to atmospheric aerosol, *Chem. Rev.*, 119, 3472–
552 3509, <https://doi.org/10.1021/acs.chemrev.8b00395>, 2019.

553 Brown, S. S. and Stutz, J.: Nighttime radical observations and chemistry, *Chem. Soc. Rev.*, 41, 6405–6447,
554 <https://doi.org/10.1039/C2CS35181A>, 2012.

555 Canagaratna, M. R., Jayne, J. T., Jimenez, J. L., Allan, J. D., Alfarra, M. R., Zhang, Q., Onasch, T. B., Drewnick,
556 F., Coe, H., Middlebrook, A., Delia, A., Williams, L. R., Trimborn, A. M., Northway, M. J., DeCarlo, P. F.,
557 Kolb, C. E., Davidovits, P., and Worsnop, D. R.: Chemical and microphysical characterization of ambient
558 aerosols with the Aerodyne aerosol mass spectrometer, *Mass Spectrom. Rev.*, 26, 185–222,
559 <https://doi.org/10.1002/mas.20115>, 2007.

560 Canagaratna, M. R., Jimenez, J. L., Kroll, J. H., Chen, Q., Kessler, S. H., Massoli, P., Hildebrandt Ruiz, L., Fortner,
561 E., Williams, L. R., Wilson, K. R., Surratt, J. D., Donahue, N. M., Jayne, J. T., and Worsnop, D. R.: Elemental

562 ratio measurements of organic compounds using aerosol mass spectrometry: Improved sensitivity and
563 intercomparability, *Atmos. Chem. Phys.*, 15, 253–272, <https://doi.org/10.5194/acp-15-253-2015>, 2015.

564 Cao, L.-M., Huang, X.-F., Li, Y.-Y., Hu, M., and He, L.-Y.: Volatility measurement of atmospheric submicron
565 aerosols in an urban atmosphere in southern China, *Atmos. Chem. Phys.*, 18, 1729–1743,
566 <https://doi.org/10.5194/acp-18-1729-2018>, 2018.

567 Cappa, C. D. and Jimenez, J. L.: Quantitative estimates of the volatility of ambient organic aerosol, *Atmos. Chem.*
568 *Phys.*, 10, 5409–5424, <https://doi.org/10.5194/acp-10-5409-2010>, 2010.

569 Chen, Y., Wang, Z., Wang, Y., Zheng, X., Fu, P., Kawamura, K., and Zhang, Y.: Characterization of nitrogen-
570 containing organic aerosol in Guangzhou, China: seasonal variation, formation mechanism and source
571 apportionment, *Atmos. Chem. Phys.*, 21, 4329–4344, <https://doi.org/10.5194/acp-21-4329-2021>, 2021.

572 Chhabra, P. S., Ng, N. L., Canagaratna, M. R., Corrigan, A. L., Russell, L. M., Worsnop, D. R., Goldstein, A. H.,
573 and Seinfeld, J. H.: Elemental composition and oxidation of chamber organic aerosol, *Atmos. Chem. Phys.*, 11,
574 8827–8841, <https://doi.org/10.5194/acp-11-8827-2011>, 2011.

575 Cubison, M. J., Ortega, A. M., Hayes, P. L., Farmer, D. K., Day, D., Lechner, M. J., Burt, H. J., Allan, J. D., Blake,
576 D. R., Jimenez, J. L., and Worsnop, D. R.: Effects of aging on organic aerosol from open biomass burning
577 smoke in aircraft and laboratory studies, *Atmos. Chem. Phys.*, 11, 12049–12064, <https://doi.org/10.5194/acp-11-12049-2011>, 2011.

578 D'Ambro, E. L., Schobesberger, S., Gaston, C. J., Lopez-Hilfiker, F. D., Mohr, C., Iyer, S., Kurtén, T., Thornton,
579 J. A., and Ehn, M.: Molecular composition and volatility of isoprene photochemical oxidation secondary
580 organic aerosol under low- and high-NO_x conditions, *Atmos. Chem. Phys.*, 17, 159–174,
581 <https://doi.org/10.5194/acp-17-159-2017>, 2017.

582 DeCarlo, P. F., Kimmel, J. R., Trimborn, A., Northway, M. J., Jayne, J. T., Aiken, A. C., Gonin, M., Fuhrer, K.,
583 Horvath, T., Docherty, K. S., Worsnop, D. R., and Jimenez, J. L.: Field-deployable, high-resolution, time-of-
584 flight aerosol mass spectrometer, *Anal. Chem.*, 78, 8281–8289, <https://doi.org/10.1021/ac061249>, 2006.

585 Donahue, N. M., Robinson, A. L., Stanier, C. O., and Pandis, S. N.: Coupled partitioning, dilution, and chemical
586 aging of semivolatile organics, *Environ. Sci. Technol.*, 40, 2635–2643, <https://doi.org/10.1021/es052297c>,
587 2006.

588 Donahue, N. M., Robinson, A. L., and Pandis, S. N.: Atmospheric organic particulate matter: From smoke to
589 secondary organic aerosol, *Atmos. Environ.*, 43, 94–106, <https://doi.org/10.1016/j.atmosenv.2008.09.055>,
590 2009.

592 Donahue, N. M., Epstein, S. A., Pandis, S. N., and Robinson, A. L.: A two-dimensional volatility basis set – Part
593 1: Organic-aerosol mixing thermodynamics, *Atmos. Chem. Phys.*, 11, 3303–3318, <https://doi.org/10.5194/acp-11-3303-2011>, 2011.

594

595 Ehn, M., Thornton, J. A., Kleist, E., Sipilä, M., Junninen, H., Pullinen, I., Springer, M., Rubach, F., Tillmann, R.,
596 Schreiber, B., Wendisch, M., Wahner, A., Mentel, T. F., Worsnop, D. R., and Kulmala, M.: A large source of
597 low-volatility secondary organic aerosol, *Nature*, 506, 476–479, <https://doi.org/10.1038/nature13032>, 2014.

598 EPA: *EPA Positive Matrix Factorization (PMF) 5.0 Fundamentals and User Guide*, U.S. Environmental Protection
599 Agency, Office of Research and Development, Washington, DC, EPA/600/R-14/108, 2014.

600 Faulhaber, A. E., Thomas, B. M., Jimenez, J. L., Jayne, J. T., Worsnop, D. R., and Ziemann, P. J.: Characterization
601 of a thermodenuder–particle beam mass spectrometer system for the study of organic aerosol volatility and
602 composition, *Atmos. Meas. Tech.*, 2, 15–31, <https://doi.org/10.5194/amt-2-15-2009>, 2009.

603 Feng, T., Wang, Y., Hu, W., Zhu, M., Song, W., Chen, W., Wu, Z., Lou, S., Huang, C., Wang, X., and Wang, X.:
604 Impact of aging on the sources, volatility, and viscosity of organic aerosols in Chinese outflows, *Atmos. Chem.
605 Phys.*, 23, 611–636, <https://doi.org/10.5194/acp-23-611-2023>, 2023.

606 Ge, X., Wexler, A. S., and Clegg, S. L.: Atmospheric amines – Part I. A review, *Atmos. Environ.*, 45, 524–546,
607 <https://doi.org/10.1016/j.atmosenv.2010.10.012>, 2011a.

608 Ge, X., Wexler, A. S., and Clegg, S. L.: Atmospheric amines – Part II. Thermodynamic properties and gas-particle
609 partitioning, *Atmos. Chem. Phys.*, 11, 55–69, <https://doi.org/10.5194/acp-11-55-2011>, 2011b.

610 Ge, X., Wexler, A. S., and Clegg, S. L.: Atmospheric amines – Part III: Photochemistry and toxicity, *Atmos.
611 Environ.*, 45, 561–591, <https://doi.org/10.1016/j.atmosenv.2010.11.050>, 2011c.

612 Ghim, Y. S., Moon, K.-C., Lee, S., and Kim, Y. P.: Visibility trends in Korea during the past two decades, *J. Air
613 Waste Manag. Assoc.*, 55, 73–82, <https://doi.org/10.1080/10473289.2005.10464599>, 2005.

614 Gil, J., Lee, Y., and Kim, Y. P.: Characteristics of HONO and its impact on O₃ formation in the Seoul Metropolitan
615 Area during KORUS-AQ, *Atmos. Environ.*, 246, 118032, <https://doi.org/10.1016/j.atmosenv.2020.118032>,
616 2021.

617 Glasius, M. and Goldstein, A. H.: Recent discoveries and future challenges in atmospheric organic chemistry,
618 *Environ. Sci. Technol.*, 50, 2754–2764, <https://doi.org/10.1021/acs.est.5b05105>, 2016.

619 Grieshop, A. P., Logue, J. M., Donahue, N. M., and Robinson, A. L.: Laboratory investigation of photochemical
620 oxidation of organic aerosol from wood fires 1: Measurement and simulation of organic aerosol evolution,
621 *Atmos. Chem. Phys.*, 9, 1263–1277, <https://doi.org/10.5194/acp-9-1263-2009>, 2009.

622 Hallquist, M., Wenger, J. C., Baltensperger, U., Rudich, Y., Simpson, D., Claeys, M., Dommen, J., Donahue, N.
623 M., George, C., Goldstein, A. H., Hamilton, J. F., Herrmann, H., Hoffmann, T., Iinuma, Y., Jang, M., Jenkin,
624 M. E., Jimenez, J. L., Kiendler-Scharr, A., Maenhaut, W., McFiggans, G., Mentel, Th. F., Monod, A., Prévôt,
625 A. S. H., Seinfeld, J. H., Surratt, J. D., Szmigielski, R., and Wildt, J.: The formation, properties and impact of
626 secondary organic aerosol: current and emerging issues, *Atmos. Chem. Phys.*, 9, 5155–5236,
627 <https://doi.org/10.5194/acp-9-5155-2009>, 2009.

628 Hamanaka, R. B. and Mutlu, G. M.: Particulate matter air pollution: Effects on the cardiovascular system, *Front.
629 Endocrinol.*, 9, 680, <https://doi.org/10.3389/fendo.2018.00680>, 2018.

630 Han, K.-M., Kim, D.-G., Kim, J., Lee, S., Song, C.-H., Kim, P. S., Kim, J., Lim, H., and Kim, Y.: Crop residue
631 burning emissions and impact on particulate matter over South Korea, *Atmosphere*, 13, 559,
632 <https://doi.org/10.3390/atmos13040559>, 2022.

633 Hanson, D. R., McMurry, P. H., Jiang, J., Tanner, D., and Huey, L. G.: Ambient pressure proton transfer mass
634 spectrometry: detection of amines and ammonia, *Environ. Sci. Technol.*, 45, 8881–8888,
635 <https://doi.org/10.1021/es2018817>, 2011.

636 Hayes, P. L., Ortega, A. M., Cubison, M. J., Froyd, K. D., Zhao, Y., Cliff, S. S., Hu, W. W., Toohey, D. W., Flynn,
637 J. H., Lefer, B. L., Grossberg, N., Alvarez, S., Rappenglück, B., Taylor, J. W., Allan, J. D., Holloway, J. S.,
638 Gilman, J. B., Kuster, W. C., de Gouw, J. A., Massoli, P., Zhang, X., Canagaratna, M. R., Zotter, P., Prévôt,
639 A. S. H., Washenfelder, R. A., Young, D. J., Kriner, A. J., and Jimenez, J. L.: Organic aerosol composition and
640 sources in Pasadena, California, during the 2010 CalNex campaign, *J. Geophys. Res.-Atmos.*, 118, 9233–9257,
641 <https://doi.org/10.1002/jgrd.50530>, 2013.

642 He, L.-Y., Lin, Y., Huang, X. F., Guo, W. W., Niu, J. L., Shen, Y. F., Sen, J., and Hu, M.: Characterization of high-
643 resolution aerosol mass spectra of primary organic aerosol emissions from Chinese cooking and biomass
644 burning, *Atmos. Chem. Phys.*, 10, 11535–11543, <https://doi.org/10.5194/acp-10-11535-2010>, 2010

645 Hennigan, C. J., Sullivan, A. P., Collett Jr., J. L., and Robinson, A. L.: Levoglucosan stability in biomass burning
646 particles exposed to hydroxyl radicals, *Geophys. Res. Lett.*, 37, L09806,
647 <https://doi.org/10.1029/2010GL043088>, 2010.

648 Huang, X.-F., He, L.-Y., Hu, M., Canagaratna, M. R., Sun, Y., Zhang, Q., and Worsnop, D. R.: Highly time-
649 resolved chemical characterization of atmospheric submicron particles during 2008 Beijing Olympic Games
650 using an Aerodyne High-Resolution Aerosol Mass Spectrometer, *Atmos. Chem. Phys.*, 10, 8933–8945,
651 <https://doi.org/10.5194/acp-10-8933-2010>, 2010.

652 Huffman, J. A., Ziemann, P. J., Jayne, J. T., Worsnop, D. R., and Jimenez, J. L.: Development and characterization
653 of a fast-stepping thermodenuder for chemically resolved aerosol volatility measurements, *Aerosol Sci.*
654 *Technol.*, 42, 395–407, <https://doi.org/10.1080/02786820802104981>, 2008.

655 Huffman, J. A., Docherty, K. S., Aiken, A. C., Cubison, M. J., Ulbrich, I. M., DeCarlo, P. F., Jayne, J. T., Worsnop,
656 D. R., Ziemann, P. J., and Jimenez, J. L.: Chemically-resolved aerosol volatility measurements from two
657 megacity field studies, *Atmos. Chem. Phys.*, 9, 7161–7182, <https://doi.org/10.5194/acp-9-7161-2009>, 2009.

658 IPCC: *Climate Change 2021: The Physical Science Basis*. Contribution of Working Group I to the Sixth
659 Assessment Report of the Intergovernmental Panel on Climate Change, edited by: Masson-Delmotte, V., Zhai,
660 P., Pirani, A., Connors, S. L., Péan, C., Berger, S., Caud, N., Chen, Y., Goldfarb, L., Gomis, M. I., Huang, M.,
661 Leitzell, K., Lonnoy, E., Matthews, J. B. R., Maycock, T. K., Waterfield, T., Yelekçi, O., Yu, R., and Zhou,
662 B., Cambridge University Press, Cambridge, UK and New York, NY, USA, 817–922,
663 <https://doi.org/10.1017/9781009157896.008>, 2021.

664 Jeon, J., Chen, Y., and Kim, H.: Influence of meteorology on emission sources and physicochemical properties of
665 particulate matter in Seoul, Korea during heating period, *Atmos. Environ.*, 301, 119733,
666 <https://doi.org/10.1016/j.atmosenv.2023.119733>, 2023.

667 Jiang, F., Liu, Q., Huang, X., Wang, T., Zhuang, B., and Xie, M.: Regional modelling of secondary organic aerosol
668 over China using WRF/Chem, *J. Aerosol Sci.*, 53, 50–61, <https://doi.org/10.1016/j.jaerosci.2011.09.003>, 2012.

669 Jimenez, J. L., Canagaratna, M. R., Donahue, N. M., Prevot, A. S. H., Zhang, Q., Kroll, J. H., DeCarlo, P. F., Allan,
670 J. D., Coe, H., Ng, N. L., Aiken, A. C., Docherty, K. S., Ulbrich, I. M., Grieshop, A. P., Robinson, A. L.,
671 Duplissy, J., Smith, J. D., Wilson, K. R., Lanz, V. A., Hueglin, C., Sun, Y. L., Tian, J., Laaksonen, A.,
672 Raatikainen, T., Rautiainen, J., Vaattovaara, P., Ehn, M., Kulmala, M., Tomlinson, J. M., Collins, D. R.,
673 Cubison, M. J., Dunlea, E. J., Huffman, J. A., Onasch, T. B., Alfarra, M. R., Williams, P. I., Bower, K., Kondo,
674 Y., Schneider, J., Drewnick, F., Borrmann, S., Weimer, S., Demerjian, K., Salcedo, D., Cottrell, L., Griffin, R.,
675 J., Rautianen, J., and Worsnop, D. R.: Evolution of organic aerosols in the atmosphere, *Science*, 326, 1525–
676 1529, <https://doi.org/10.1126/science.1180353>, 2009.

677 Kang, H. G., Kim, Y., Collier, S., Zhang, Q., and Kim, H.: Volatility of springtime ambient organic aerosol derived
678 with thermodenuder aerosol mass spectrometry in Seoul, Korea, *Environ. Pollut.*, 310, 119203,
679 <https://doi.org/10.1016/j.envpol.2022.119203>, 2022.

680 Karnezi, E., Riipinen, I., and Pandis, S. N.: Measuring the atmospheric organic aerosol volatility distribution: a
681 theoretical analysis, *Atmos. Meas. Tech.*, 7, 2953–2965, <https://doi.org/10.5194/amt-7-2953-2014>, 2014.

682

683 Kim, H., Zhang, Q., Bae, G.-N., Kim, J. Y., and Lee, S. B.: Sources and atmospheric processing of winter aerosols
684 in Seoul, Korea: Insights from real-time measurements using a high-resolution aerosol mass spectrometer,
685 *Atmos. Chem. Phys.*, 17, 2009–2033, <https://doi.org/10.5194/acp-17-2009-2017>, 2017.

686 Kim, H., Zhang, Q., Sun, Y., Bae, G. N., Lee, B. E., Park, K., and Kim, Y. J.: Measurement report: Characterization
687 of severe spring haze episodes and influences of long-range transport in the Seoul metropolitan area in March
688 2019, *Atmos. Chem. Phys.*, 20, 11527–11545, <https://doi.org/10.5194/acp-20-11527-2020>, 2020.

689 Kim, K., Park, R., Lee, Y., Kim, S., Gil, J., Jeong, J. I., and Kim, Y. P.: An investigation into atmospheric nitrous
690 acid (HONO) and its sources in East Asia, *Atmos. Chem. Phys.*, 24, 12575–12593, <https://doi.org/10.5194/acp-24-12575-2024>, 2024.

692 Kroll, J. H. and Seinfeld, J. H.: Chemistry of secondary organic aerosol: Formation and evolution of low-volatility
693 organics in the atmosphere, *Atmos. Environ.*, 42, 3593–3624, <https://doi.org/10.1016/j.atmosenv.2008.01.003>,
694 2008.

695 Kroll, J. H., Smith, J. D., Che, D. L., Kessler, S. H., Worsnop, D. R., and Wilson, K. R.: Measurement of
696 fragmentation and functionalization pathways in the heterogeneous oxidation of organic aerosol, *Environ. Sci.
697 Technol.*, 43, 7826–7833, <https://doi.org/10.1021/es901683r>, 2009.

698 Kroll, J. H., Donahue, N. M., Jimenez, J. L., Kessler, S. H., Canagaratna, M. R., Wilson, K. R., Altieri, K. E.,
699 Mazzoleni, L. R., Wozniak, A. S., Bluhm, H., Mysak, E. R., Smith, J. D., Kolb, C. E., and Worsnop, D. R.:
700 Carbon oxidation state as a metric for describing the chemistry of atmospheric organic aerosol, *Nat. Chem.*, 3,
701 133–139, <https://doi.org/10.1038/nchem.948>, 2011.

702 Kwon, S., Won, S. R., Lim, H. B., Jang, K. S., and Kim, H.: Relationship between PM1.0 and PM2.5 in urban and
703 background areas of the Republic of Korea, *Atmos. Pollut. Res.*, 14, 101858,
704 <https://doi.org/10.1016/j.apr.2023.101858>, 2023.

705 Lamb, K. D., Kim, B.-G., and Kim, S.-W.: Estimating source-region influences on black carbon in South Korea
706 using the BC/CO ratio, *J. Geophys. Res.-Atmos.*, 123, 11579–11591, <https://doi.org/10.1029/2018JD029257>,
707 2018.

708 Lambe, A. T., Onasch, T. B., Massoli, P., Croasdale, D. R., Wright, J. P., Ahern, A. T., Williams, L. R., Worsnop,
709 D. R., and Davidovits, P.: Transitions from Functionalization to Fragmentation Reactions of Laboratory
710 Secondary Organic Aerosol (SOA) Generated from the OH Oxidation of Alkane Precursors, *Environ. Sci.
711 Technol.*, 46, 5430–5437, <https://doi.org/10.1021/es300274t>, 2012.

712 Li, J., Zhang, M., Wu, F., Sun, Y., and Tang, G.: Assessment of the impacts of aromatic VOC emissions and yields
713 of SOA on SOA concentrations with the air quality model RAMS-CMAQ, *Atmos. Environ.*, 158, 105–115,
714 <https://doi.org/10.1016/j.atmosenv.2017.03.035>, 2017.

715 López-Hilfiker, F. D., Mohr, C., Ehn, M., Voigtlander, J., Abrahamsson, K., Hallquist, M., Bertman, S. B.,
716 Kjærgaard, H. G., and Thornton, J. A.: A novel method for online analysis of gas and particle composition:
717 description and evaluation of a Filter Inlet for Gases and AEROsols (FIGAERO), *Atmos. Meas. Tech.*, 7, 983–
718 1001, <https://doi.org/10.5194/amt-7-983-2014>, 2014.

719 López-Hilfiker, F. D., Mohr, C., Ehn, M., Voigtlander, J., Abrahamsson, K., Hallquist, M., Bertman, S. B.,
720 Kjærgaard, H. G., and Thornton, J. A.: Molecular composition and volatility of organic aerosol in the
721 Southeastern U.S. using FIGAERO–CIMS with comparison to AMS, *Environ. Sci. Technol.*, 50, 2200–2209,
722 <https://doi.org/10.1021/acs.est.5b04769>, 2016.

723 Manosalidis, I., Stavropoulou, E., Starvropoulos, A., and Bezirtzoglou, E.: Environmental and health impacts of air
724 pollution: a review, *Front. Public Health*, 8, 14, <https://doi.org/10.3389/fpubh.2020.00014>, 2020.

725 Mao, J., Wang, L., Lu, C., Liu, J., Li, M., Tang, G., Ji, D., Zhang, S., and Wang, Y.: High-resolution modeling of
726 gaseous methylamines over a polluted region in China: source-dependent emissions and implications of spatial
727 variations, *Atmos. Chem. Phys.*, 18, 7933–7950, <https://doi.org/10.5194/acp-18-7933-2018>, 2018.

728 Matsui, H., Koike, M., Takegawa, N., Kondo, Y., Griffin, R. J., Miyazaki, Y., Yokouchi, Y., and Ohara, T.:
729 Secondary organic aerosol formation in urban air: Temporal variations and possible contributions from
730 unidentified hydrocarbons, *J. Geophys. Res.-Atmos.*, 114, D02209, <https://doi.org/10.1029/2008JD010164>,
731 2009.

732 Mohr, C., DeCarlo, P. F., Heringa, M. F., Chirico, R., Slowik, J. G., Richter, R., Reche, C., Alastuey, A., Querol,
733 X., Seco, R., Peñuelas, J., Jiménez, J. L., Crippa, M., Zimmermann, R., Baltensperger, U., and Prévôt, A. S.
734 H.: Identification and quantification of organic aerosol from cooking and other sources in Barcelona using
735 aerosol mass spectrometer data, *Atmos. Chem. Phys.*, 12, 1649–1665, <https://doi.org/10.5194/acp-12-1649-2012>, 2012.

737 Nault, B. A., Campuzano-Jost, P., Day, D. A., Schroder, J. C., Young, D. E., Hu, W. W., Handschy, A. V., Jo, D.
738 S., Cohen, R. C., Wooldridge, P. J., Giovane, L. G., and Jimenez, J. L.: Secondary organic aerosol production
739 from local emissions dominates over Seoul during KORUS-AQ, *Atmos. Chem. Phys.*, 18, 17769–17800,
740 <https://doi.org/10.5194/acp-18-17769-2018>, 2018.

741 Ng, N. L., Canagaratna, M. R., Zhang, Q., Jimenez, J. L., Tian, J., Ulbrich, I. M., Kroll, J. H., Docherty, K. S.,
742 Chhabra, P. S., Bahreini, R., Murphy, S. M., Seinfeld, J. H., Hildebrandt, L., Donahue, N. M., DeCarlo, P. F.,

743 Lanz, V. A., Prévôt, A. S. H., Dinar, E., Rudich, Y., and Worsnop, D. R.: Organic aerosol components observed
744 in Northern Hemispheric datasets from Aerosol Mass Spectrometry, *Atmos. Chem. Phys.*, 10, 4625–4641,
745 <https://doi.org/10.5194/acp-10-4625-2010>, 2010.

746 Nielsen, C. J., Herrmann, H., and Weller, C.: Atmospheric chemistry and environmental impact of the use of amines
747 in carbon capture and storage (CCS), *Chem. Soc. Rev.*, 41, 6684–6704, <https://doi.org/10.1039/C2CS35059A>,
748 2012.

749 Paatero, P. and Tapper, U.: Positive matrix factorization – A nonnegative factor model with optimal utilization of
750 error estimates of data values, *Environmetrics*, 5, 111–126, <https://doi.org/10.1002/env.3170050203>, 1994.

751 Paciga, A., Young, D. E., Ward, M. W., Gkatzoflias, D., and Pandis, S. N.: Volatility of organic aerosol and its
752 components in the megacity of Paris, *Atmos. Chem. Phys.*, 16, 2013–2031, <https://doi.org/10.5194/acp-16-2013-2016>, 2016.

753 Riipinen, I., Pierce, J. R., Donahue, N. M., and Pandis, S. N.: Equilibration time scales of organic aerosol inside
754 thermodenuders: Kinetics versus equilibrium thermodynamics, *Atmos. Environ.*, 44, 597–607,
755 <https://doi.org/10.1016/j.atmosenv.2009.11.022>, 2010.

756 Robinson, A. L., Donahue, N. M., Shrivastava, M. K., Weitkamp, E. A., Sage, A. M., Grieshop, A. P., Lane, T. E.,
757 Pierce, J. R., and Pandis, S. N.: Rethinking organic aerosols: Semivolatile emissions and photochemical aging,
758 *Science*, 315, 1259–1262, <https://doi.org/10.1126/science.1133061>, 2007.

759 Rovelli, G., Miles, R. E. H., Reid, J. P., and Clegg, S. L.: Hygroscopic properties of aminium sulfate aerosols,
760 *Atmos. Chem. Phys.*, 17, 4369–4385, <https://doi.org/10.5194/acp-17-4369-2017>, 2017.

761 Saarikoski, S., Carbone, S., Decesari, S., Julianelli, L., Angelini, F., Canagaratna, M. R., Ng, N. L., Trimborn,
762 A., Facchini, M. C., Fuzzi, S., Hillamo, R., and Worsnop, D. R.: Chemical characterization of springtime
763 submicrometer aerosol in Po Valley, Italy, *Atmos. Chem. Phys.*, 12, 8401–8421, <https://doi.org/10.5194/acp-12-8401-2012>, 2012.

764 Saha, P. K., Khlystov, A., and Grieshop, A. P.: Determining aerosol volatility parameters using a “dual
765 thermodenuder” system: Application to laboratory-generated organic aerosols, *Aerosol Sci. Technol.*, 49, 620–
766 632, <https://doi.org/10.1080/02786826.2015.1056769>, 2014.

767 Scott, W. D. and Cattell, F. C. R.: Vapor pressure of ammonium sulfates, *Atmos. Environ.*, 13, 987–1000,
768 [https://doi.org/10.1016/0004-6981\(79\)90174-4](https://doi.org/10.1016/0004-6981(79)90174-4), 1979.

769 Silva, P. J., Erupe, M. E., Price, D., Elias, J., Malloy, Q. G. J., Li, Q., Warren, B., and Cocker III, D. R.:
770 Trimethylamine as precursor to secondary organic aerosol formation via nitrate radical reaction in the
771 atmosphere, *Environ. Sci. Technol.*, 42, 4689–4696, <https://doi.org/10.1021/es703016v>, 2008.

772

773

774 Simoneit, B. R. T.: Biomass burning – a review of organic tracers for smoke from incomplete combustion, *Appl.*
775 *Geochem.*, 17, 129–162, [https://doi.org/10.1016/S0883-2927\(01\)00061-0](https://doi.org/10.1016/S0883-2927(01)00061-0), 2002.

776 Sinha, A., George, I., Holder, A., Preston, W., Hays, M., and Grieshop, A. P.: Development of volatility
777 distributions for organic matter in biomass burning emissions, *Environ. Sci. Adv.*, 3, 11–23,
778 <https://doi.org/10.1039/D2EA00080F>, 2023.

779 Slater, E. J., Gkatzolias, D., Wang, Y., Zhang, Q., and Pandis, S. N.: Elevated levels of OH observed in haze
780 events during wintertime Beijing, *Atmos. Chem. Phys.*, 20, 14847–14871, <https://doi.org/10.5194/acp-20-14847-2020>, 2020.

781 Soleimani, M., Ebrahimi, Z., Mirghaffari, N., and Naseri, M.: Source identification of polycyclic aromatic
782 hydrocarbons associated with fine particulate matters (PM2.5) in Isfahan City, Iran, using diagnostic ratio and
783 PMF model, *Environ. Sci. Pollut. Res.*, 29, 30310–30326, <https://doi.org/10.1007/s11356-021-17635-8>, 2022.

784 Sun, Y. L., Zhang, Q., Schwab, J. J., Canagaratna, M. R., Ng, N. L., Onasch, T. B., Jayne, J. T., Worsnop, D. R.,
785 and Demerjian, K. L.: Characterization of the sources and processes of organic aerosols in New York City with
786 a high-resolution time-of-flight aerosol mass spectrometer, *Atmos. Chem. Phys.*, 11, 1581–1602,
787 <https://doi.org/10.5194/acp-11-1581-2011>, 2011.

788 Sun, Y., Jiang, Q., Wang, Z., Fu, P., Li, J., Yang, T., and Yin, Y.: Investigation of the sources and evolution
789 processes of severe haze pollution in Beijing in January 2013, *J. Geophys. Res.-Atmos.*, 119, 4380–4398,
790 <https://doi.org/10.1002/2014JD021641>, 2014.

791 Tiszenkel, L., Flynn, J. H., and Lee, S.-H.: Measurement report: Urban ammonia and amines in Houston, Texas,
792 *Atmos. Chem. Phys.*, 24, 11351–11363, <https://doi.org/10.5194/acp-24-11351-2024>, 2024.

793 Ulbrich, I. M., Canagaratna, M. R., Zhang, Q., Worsnop, D. R., and Jimenez, J. L.: Interpretation of organic
794 components from Positive Matrix Factorization of aerosol mass spectrometric data, *Atmos. Chem. Phys.*, 9,
795 2891–2918, <https://doi.org/10.5194/acp-9-2891-2009>, 2009.

796 Waked, A., Favez, O., Alleman, L. Y., Piot, C., Petit, J. E., Delaunay, T., Verlinden, E., Jayne, J., and Sciare, J.:
797 Source apportionment of PM10 in a north-western Europe regional urban background site (Lens, France) using
798 positive matrix factorization and including primary emissions, *Atmos. Chem. Phys.*, 14, 3325–3346,
799 <https://doi.org/10.5194/acp-14-3325-2014>, 2014.

800 Xu, L., Kollman, M. S., Song, C., Shilling, J. E., and Ng, N. L.: Effects of NO_x on the volatility of secondary
801 organic aerosol from isoprene photooxidation, *Environ. Sci. Technol.*, 48, 2253–2262,
802 <https://doi.org/10.1021/es404842g>, 2014.

804 Xu, L., Williams, L. R., Young, D. E., Allan, J. D., Coe, H., Massoli, P., Fortner, E., Chhabra, P., Herndon, S.,
805 Brooks, W. A., Jayne, J. T., Worsnop, D. R., Aiken, A. C., Liu, S., Gorkowski, K., Dubey, M. K., Fleming, Z.
806 L., Visser, S., Prévôt, A. S. H., and Ng, N. L.: Wintertime aerosol chemical composition, volatility, and spatial
807 variability in the Greater London Area, *Atmos. Chem. Phys.*, 16, 1139–1160, <https://doi.org/10.5194/acp-16-1139-2016>, 2016.

808

809 Xu, W., Sun, Y., Wang, Q., Chen, C., Chen, J., Ge, X., Zhang, Q., Ji, D., Du, W., Zhao, J., Zhou, W., and Worsnop,
810 D. R.: Seasonal characterization of organic nitrogen in atmospheric aerosols using high-resolution aerosol mass
811 spectrometry in Beijing, China, *ACS Earth Space Chem.*, 1, 649–658,
812 <https://doi.org/10.1021/acsearthspacechem.7b00106>, 2017.

813 Xu, W., Xie, C., Karnezi, E., Zhang, Q., Wang, J., Pandis, S. N., Ge, X., Zhang, J., An, J., Wang, Q., Zhao, J., Du,
814 W., and Sun, Y.: Summertime aerosol volatility measurements in Beijing, China, *Atmos. Chem. Phys.*, 19,
815 10205–10216, <https://doi.org/10.5194/acp-19-10205-2019>, 2019.

816 Xu, W., Takeuchi, M., Chen, C., Qiu, Y., Xie, C., Xu, W., Ma, N., Worsnop, D. R., Ng, N. L., and Sun, Y.:
817 Estimation of particulate organic nitrates from thermodenuder–aerosol mass spectrometer measurements in the
818 North China Plain, *Atmos. Meas. Tech.*, 14, 3693–3705, <https://doi.org/10.5194/amt-14-3693-2021>, 2021.

819 Yao, L., Wang, M. Y., Wang, X. K., Zhang, W. Q., Liu, Y., Li, L., Liu, Y. J., and Li, S. M.: Atmospheric new
820 particle formation from sulfuric acid and amines in a Chinese megacity, *Sci. Bull.*, 61, 939–945,
821 <https://doi.org/10.1007/s11434-016-1083-0>, 2016.

822 Yoo, H., Lee, H., and Kim, Y. P.: Insights from single-particle analysis: submicron aerosol composition in Seoul
823 during KORUS-AQ, *Atmos. Chem. Phys.*, 24, 853–872, <https://doi.org/10.5194/acp-24-853-2024>, 2024.

824 You, Y., Renbaum-Wolff, L., Carreras-Sospedra, M., Dabdub, D., Bertram, A. K., Martin, S. T., and Smith, J. D.:
825 Images reveal that amines promote the heterogeneous reaction of epoxides in model organic aerosols, *J. Phys.*
826 *Chem. Lett.*, 5, 3211–3215, <https://doi.org/10.1021/jz501268k>, 2014.

827 Zhang, Q., Alfarra, M. R., Worsnop, D. R., Allan, J. D., Coe, H., Canagaratna, M. R., and Jimenez, J. L.:
828 Deconvolution and quantification of hydrocarbon-like and oxygenated organic aerosols based on aerosol mass
829 spectrometry, *Environ. Sci. Technol.*, 39, 4938–4952, <https://doi.org/10.1021/es0485681>, 2005.

830 Zhang, Q., Jimenez, J. L., Canagaratna, M. R., Allan, J. D., Coe, H., Ulbrich, I., Alfarra, M. R., Takami, A.,
831 Middlebrook, A. M., Sun, Y. L., Dzepina, K., Dunlea, E., Docherty, K., DeCarlo, P., Salcedo, D., Onasch, T.
832 B., Jayne, J. T., Miyoshi, T., Shimono, A., Hatakeyama, N., Takegawa, N., Kondo, Y., Schneider, J., Drewnick,
833 F., Weimer, S., Demerjian, K. L., Williams, P. I., Bower, K. N., Bahreini, R., Cottrell, L., Griffin, R. J.,
834 Rautianen, J., and Worsnop, D. R.: Ubiquity and dominance of oxygenated species in organic aerosols in

835 anthropogenically-influenced Northern Hemisphere mid-latitudes, *Geophys. Res. Lett.*, 34, L13801,
836 <https://doi.org/10.1029/2007GL029979>, 2007.

837 Zhang, Q., Jimenez, J. L., Canagaratna, M. R., Ulbrich, I. M., Ng, N. L., Worsnop, D. R., and Sun, Y.:
838 Understanding atmospheric organic aerosols via factor analysis of aerosol mass spectrometry: A review, *Anal.
839 Bioanal. Chem.*, 401, 3045–3067, <https://doi.org/10.1007/s00216-011-5355-y>, 2011.

840 Zhao, B., Wang, S., Donahue, N. M., Jathar, S. H., Huang, X., Wu, W., Hao, J., and Jimenez, J. L.: Quantifying
841 the effect of organic aerosol aging and intermediate-volatility emissions on regional-scale aerosol pollution in
842 China, *Sci. Rep.*, 6, 28815, <https://doi.org/10.1038/srep28815>, 2016.

843 Zhao, H., Che, H., Zhang, X., Ma, Y., Wang, Y., Wang, H., and Wang, Y.: Characteristics of visibility and
844 particulate matter (PM) in an urban area of Northeast China, *Atmos. Pollut. Res.*, 4, 427–434,
845 <https://doi.org/10.5094/APR.2013.049>, 2013.

846 Zhou, S., Collier, S., Jaffe, D. A., Briggs, N. L., Hee, J., Sedlacek III, A. J., Kleinman, L., and Lewis, K.: Regional
847 influence of wildfires on aerosol chemistry in the western US and insights into atmospheric aging of biomass
848 burning organic aerosol, *Atmos. Chem. Phys.*, 17, 2477–2493, <https://doi.org/10.5194/acp-17-2477-2017>,
849 2017.

850 Ziemann, P. J. and Atkinson, R.: Kinetics, products, and mechanisms of secondary organic aerosol formation from
851 gas-phase reactions of organic compounds, *Chem. Soc. Rev.*, 41, 6582–6605,
852 <https://doi.org/10.1039/C2CS35122F>, 2012.